JAERI-RESEARCH-98-040
FERMILAB
SEP 16 1998
Fermilab Library
0 1160 0067549 0

JAERI-Research
98-040

NEUTRON DATA EVALUATION OF ^{238}U

August 1998

NAME | DATE | M.S.
RETURN TO FERMILAB LIBRARY

V. M. MASLOV*, Yu. V. PORODZINSKIJ*,
Akira HASEGAWA and Keiichi SHIBATA

日本原子力研究所
Japan Atomic Energy Research Institute

本レポートは，日本原子力研究所が不定期に公刊している研究報告書です。
入手の問合わせは，日本原子力研究所研究情報部研究情報課（〒319-1195　茨城県那珂郡東海村）あて，お申し越しください。なお，このほかに財団法人原子力弘済会資料センター（〒319-1195　茨城県那珂郡東海村日本原子力研究所内）で複写による実費頒布をおこなっております。

This report is issued irregularly.
Inquiries about availability of the reports should be addressed to Research Information Division, Department of Intellectual Resources, Japan Atomic Energy Research Institute, Tokai-mura, Naka-gun, Ibaraki-ken, 319-1195, Japan.

© Japan Atomic Energy Research Institute, 1998

編集兼発行　　日本原子力研究所

JAERI-Research 98-040

Neutron Data Evaluation of ^{238}U

V. M. MASLOV*※, Yu. V. PORODZINSKIJ*,
Akira HASEGAWA and Keiichi SHIBATA

Department of Nuclear Energy System
Tokai Research Establishment
Japan Atomic Energy Research Institute
Tokai-mura, Naka-gun, Ibaraki-ken

(Received July 9, 1998)

Cross sections for neutron-induced reactions on ^{238}U are calculated by using the Hauser-Feshbach-Moldauer theory, the coupled channel model and the double-humped fission barrier model. The direct excitation of ground state band levels is calculated with a rigid rotator model. The direct excitation of vibrational octupole and $K=2^+$ quadrupole bands is included using a soft (deformable) rotator model. The competition of inelastic scattering to fission reaction is shown to be sensitive to the target nucleus level density at excitations above the pairing gap. As for fission, (n,2n), (n,3n), and (n,4n) reactions, secondary neutron spectra data are consistently reproduced. Pre-equilibrium emission of first neutron is included. Shell effects in the level densities are shown to be important for estimation of energy dependence of non-emissive fission cross section.

Keywords: Evaluation, Neutron Data, ^{238}U, Statistical Model, Cross Section, Spectrum

* Radiation Physics and Chemistry Problems Institute, Minsk, Belarus
※ Visiting Researcher

^{238}Uの中性子核データの評価

日本原子力研究所東海研究所エネルギーシステム研究部
V.M. MASLOV*※・Yu.V.PORODZINSKIJ*・長谷川　明・柴田　恵一

(1998年7月9日受理)

^{238}Uの中性子誘起反応断面積を Hauser-Feshbach-Moldauer 理論、チャンネル結合模型、二山核分裂障壁模型を用いて計算した。基底状態バンドの直接励起は剛回転体模型で計算した。振動八重極及びK＝2^{+} の四重極バンドの直接励起は軟回転体模型で計算した。非弾性散乱の核分裂反応に対する競争はペアリング・ギャップ以上の励起エネルギーでの標的核の準位密度に敏感である事が分かった。核分裂、(n,2n)、(n,3n)、(n,4n)反応に関しては、二次中性子スペクトルが統一的に再現された。最初の中性子の前平衡反応による放出が考慮された。準位密度に於ける殻効果は核分裂断面積のエネルギー依存性を評価する上で重要である事が判明した。

東海研究所　〒319－1195　茨城県那珂郡東海村白方白根2－4
＊　放射線物理・化学問題研究所、ミンスク、ベラルーシ共和国
※　外国人研究者招聘制度に基づく招聘研究員

Contents

1. Introduction 1
2. Statistical Model 2
2.1 Cross Section Formula 3
2.2 Level Density 3
3. Optical Potential 8
3.1 Total Cross Section 8
3.2 Reaction Cross Section 9
3.3 Angular Distributions 9
4. Fission Cross Section 10
4.1 Fission Channel 10
4.1.1 Fission Transmission Coefficient, Level Density and Transition State Spectrum 11
4.2 Fission Data Analysis 12
5. Inelastic Scattering 12
5.1 Neutron Channel 12
5.2 Ground State Rotational Band 13
5.3 Soft Rotator Model 14
5.3.1 Octupole Band 14
5.3.2 Quadrupole Band 15
5.4 Total Inelastic Cross Section 16
5.5 Evaluated Inelastic Scattering Cross Section of JENDL-3.2 17
6. Capture Cross Section 17
6.1 Radiative Capture Channel 18
6.2 Data Analysis 19
7. Cross Sections above Emissive Fission Threshold 20
7.1 Shell Effects in First Chance Fission Cross Section 21
7.2 Secondary Neutron Spectra 22
7.2.1 Model Calculations of (n,nx) Reaction Spectra 22
7.3 (n,xn) Reaction Cross Sections 24
8. Conclusions 25
Acknowledgements 26
References 27

目　　次

1. 序　論 …… 1
2. 統計模型 …… 2
2.1 断面積公式 …… 3
2.2 準位密度 …… 3
3. 光学ポテンシャル …… 8
3.1 全断面積 …… 8
3.2 反応断面積 …… 9
3.3 角度分布 …… 9
4. 核分裂断面積 …… 10
4.1 核分裂チャンネル …… 10
4.1.1 核分裂透過係数、準位密度及び遷移状態スペクトル …… 11
4.2 核分裂データの解析 …… 12
5. 非弾性散乱 …… 12
5.1 中性子チャンネル …… 12
5.2 基底状態回転バンド …… 13
5.3 軟回転体模型 …… 14
5.3.1 八重極バンド …… 14
5.3.2 四重極バンド …… 15
5.4 全非弾性散乱断面積 …… 16
5.5 JENDL-3.2の非弾性散乱断面積 …… 17
6. 中性子捕獲断面積 …… 17
6.1 放射捕獲チャンネル …… 18
6.2 データ解析 …… 19
7. (n, n' f) 反応のしきい値以上での断面積 …… 20
7.1 核分裂断面積に於ける殻効果 …… 21
7.2 二次中性子スペクトル …… 22
7.2.1 (n, nx)反応スペクトルの計算 …… 22
7.3 (n, xn)反応断面積 …… 24
8. 結　論 …… 25
謝　辞 …… 26
参考文献 …… 27

1 Introduction

Nuclear data of ^{238}U are very important for thermal and fast reactor calculations. Especially important are inelastic scattering cross section and secondary neutron distribution [1]. Inelastic scattering processes in ^{238}U have been a source of controversy. The neutron inelastic scattering cross sections of available evaluated data files JENDL-3.2[2], ENDF/B-VI [3], BROND-2 [4], JEF-2 [5] are discrepant in most cases. The source of discrepancies is often masked by specific evaluation approaches [6], which might be documented only scarcely. The situation is further complicated by the measured inelastic scattering data discrepancies [7]. As regards the excitation functions of discrete levels there is a systematic discrepancy of data obtained by time-of-flight method [8] and by (n,n'γ) measurements [8, 9]. The measured total inelastic scattering cross section data above $\sim$1 MeV incident neutron energy [10, 11, 12] are also somewhat discrepant. Basically previous evaluated inelastic scattering cross sections were obtained with statistical theory calculations, however procedure of normalization to measured data was applied. Consequently, the possibility of describing measured data base with Hauser-Feshbach-Moldauer statistical theory still remains uncertain. In case of ENDF/B-VI data file, the evaluation approach is a correlation of theory and experiment, while in JENDL-3.2 the calculated compound discrete level inelastic scattering components are strongly renormalized to give better agreement with measured total inelastic scattering data [6]. The JEF-2 evaluation is based essentially on the superceded version of JENDL evaluation. As distinct from the previous evaluations we proceed within full-scale Hauser-Feshbach theory, coupled channel optical model and double-humped fission barrier model. Fit to the neutron-induced fission data and consistent description of (n,2n) and (n,3n) reaction data might provide a rather sound constraint for inelastic cross section calculation.

The important item for the total inelastic scattering cross section in a few MeV incident neutron energy range is the scattering to the ^{238}U continuum levels. For this the level density modelling above the pairing gap of even-even nuclide ^{238}U is important. The competition of ^{238}U(n,γn') reaction to the "true" capture reaction (n,$\gamma\gamma$) also turns out to be dependent on the target nucleus ^{238}U level density at excitations just above the pairing gap. The pairing correlation effects are important also for describing level densities of N-odd nuclei, e.g. ^{239}U fissioning nuclide at excitation energies of a few MeV. There exist some experimental signatures which are used to test the validity of the level density model and to demonstrate the importance of the collective, pairing and shell effects. The effects of pair correlations were evidenced [13] in statistical γ-decay spectra of even-even deformed nuclide ^{192}Hg. Statistical γ-decay spectra from compound

nuclei (A=114-200), formed by neutron capture, probe the level density of the excited states below neutron binding energy. The decay probabilities of nuclear states by two-step cascades [14] demonstrate almost the same kind of structure. The step-like structure in ^{239}Pu(n,2n) reaction cross section was shown to be a consequence of threshold excitation of two-quasiparticle configurations in residual even-even nuclide ^{238}Pu [15]. We demonstrate here that one needs the sophistication of level density modelling to describe consistently the available measured data base for ^{238}U.

2 Statistical Model

Hauser-Feshbach-Moldauer statistical theory is employed for partial cross section calculations below emissive fission threshold. Fissioning and residual nuclei level densities as well as fission barrier parameters are key ingredients, involved in neutron-induced actinide cross section calculations. For calculations to be accomplished, the following procedure should be pursued. First, level density parameters are defined, using neutron resonance spacing $\langle D_{obs} \rangle$ estimates for ^{238}U, ^{237}U, ^{236}U, ^{235}U and ^{234}U target nuclides, which are formed in neutron emission cascade reactions. Constant temperature level density parameters T_o, E_o, U_c are defined by fitting cumulative number of low-lying levels of ^{239}U, ^{238}U, ^{237}U, ^{236}U, ^{235}U and ^{234}U. At incident neutron energies, when continuum levels are excited, width fluctuation correction is treated within Tepel et al. [16] approach. Cross sections, calculated with statistical theory by Tepel et al. [16] approach are matched to those calculated with Hauser-Feshbach-Moldauer statistical theory at the incident neutron energy equal to the energy of last discrete level. Then fission cross sections ^{238}U, ^{237}U, ^{236}U and ^{235}U target nuclides are calculated up to emissive fission threshold to extract fission barrier parameters. After that total, reaction and direct excitation cross sections of ground state band levels up to 20 MeV are calculated, and then neutron transmission coefficients $T_l(E)$ for the code STAPRE [17] are obtained. At last, cross sections up to 20 MeV are calculated.

A coupled channels model is adopted for the calculation of direct inelastic scattering contribution of the discrete level excitation. The direct excitation of ground state rotational band levels 0^+-2^+-4^+-6^+ is estimated within rigid rotator model, which is used also for calculation of entrance neutron transmission coefficients. To calculate the direct excitation cross sections for γ-vibration ($K^\pi = 0^+$, 2^+) as well as octupole ($K^\pi = 0^-$) band levels a soft rotator model [18] is used.

In case of fast neutron ($E \leq 6$ MeV) interaction with ^{238}U target nucleus, the main competing channels against neutron inelastic scattering are fission and radiative neutron capture. Below there is an outline of the statistical model [19, 20] employed.

2.1 Cross Section Formula

In the statistical theory of nuclear reactions the neutron-induced reaction cross section is given by

$$\sigma_{nx}(E) = \frac{\pi \lambda\!\!\!^{-2}}{2(2I+1)} \sum_{ljJ\pi} (2J+1) T_{lj}^{J\pi}(E) P_x^{J\pi}(E) S_{nx}^{ljJ\pi}, \tag{1}$$

the compound nucleus decay probability $P_x^{J\pi}$ $(x = n, f, \gamma)$ is

$$P_x^{J\pi}(E) = \frac{T_x^{J\pi}(U)}{T_f^{J\pi}(U) + T_n^{J\pi}(U) + T_\gamma^{J\pi}(U)}, \tag{2}$$

where $U = B + E$ is the excitation energy of the compound nucleus, B is the neutron binding energy, E is the incident neutron energy, $T_{lj}^{J\pi}$ are the entrance neutron transmission coefficients for the channel $(ljJ\pi)$, I is the target nucleus spin. Decay probability $P_x^{J\pi}(E)$ of the compound nucleus with excitation energy U for given spin J and parity π, depends on $T_f^{J\pi}$, $T_n^{J\pi}(U)$ and $T_\gamma^{J\pi}(U)$, transmission coefficients of the fission, neutron scattering and radiative decay channels. $S_{nx}^{ljJ\pi}$ denotes partial widths Porter-Thomas fluctuation factor. Below incident neutron energy equal to cut-off energy of discrete level spectra the neutron cross sections are calculated within Hauser-Feshbach approach with correction for width fluctuation by Moldauer [21]. For width fluctuation correction calculation only Porter-Thomas fluctuations are taken into account. Effective number of degrees of freedom for fission channel is defined at the higher fission barrier saddle as $\nu_f^{J\pi} = \mathrm{T}_f^{J\pi}/\mathrm{T}_{f\,\mathrm{max}}^{J\pi}$, where $\mathrm{T}_{f\,\mathrm{max}}^{J\pi}$ is the maximum value of the fission transmission coefficient $\mathrm{T}_f^{J\pi}$. At higher incident neutron energies the Tepel et al. [16] approach is employed; it describes cross section behavior in case of large number of open channels correctly.

2.2 Level Density

Level density is the main ingredient of statistical model calculations. Level density of fissioning, residual and compound nuclei define transmission coefficients of fission, neutron scattering and radiative decay channels. We will discuss here level densities of even-even nuclide ^{238}U and even-odd nuclide ^{239}U.

The level density description should reproduce both the average neutron resonance spacing and the observed cumulative number of levels $N^{exp}(U)$. The problem which one usually dealing with is the fair description of the cumulative number of levels $N^{exp}(U)$ with the calculated cumulative number of levels $N^{theor}(U)$. To calculate the residual nucleus ^{238}U level density at the low excitation energy, i.e. just above the last discrete level excitation energy where $N^{exp}(U) \sim N^{theor}(U)$, we employ a Gilbert-Cameron-type approach. The constant temperature approximation of

$$\rho(U) = dN(U)/dU = T^{-1}\exp((U - U_o)/T) \tag{3}$$

is extrapolated up to the matching point U_c to a phenomenological model by Ignatyuk et al.[22] with the condition

$$U_c = U_o - Tln(T\rho(U_c)). \tag{4}$$

In this approach $U_o \simeq -n\triangle_o$, where $\triangle_o$ is the pairing correlation function, $\triangle_o = 12/\sqrt{A}$, A is the mass number, $n = 0$ for even-even, 1 for odd and 2 for odd-odd nuclei, i.e., U_o has the meaning of the odd-even energy shift. The value of nuclear temperature parameter T is obtained by the matching conditions at the excitation energy U_c.

At higher energies $U > U_c$ the level densities were calculated with a phenomenological model by Ignatyuk et al. [22], which takes into account the shell, pairing and collective effects in a consistent way

$$\rho(U, J, \pi) = K_{rot}(U, J)K_{vib}(U)\rho_{qp}(U, J, \pi), \tag{5}$$

where $\rho_{qp}(U, J, \pi)$ is the quasiparticle level density and $K_{rot}(U, J)$ and $K_{vib}(U)$ are factors of rotational and vibrational enhancement of the level density. The relation (5) holds in an adiabatic approximation, when collective and intrinsic excitation contributions to the total level density $\rho(U, J, \pi)$ are factorized. In this approach the modelling of total level density

$$\rho(U) = K_{rot}(U)K_{vib}(U)\frac{\omega_{qp}(U)}{\sqrt{2\pi}\sigma} = T^{-1}\exp((U - U_o)/T) \tag{6}$$

in Gilbert-Cameron-type approach looks like a simple renormalization of quasiparticle state density $\omega_{qp}(U)$ at excitation energies $U < U_c$. Here, $\sigma^2 = F_{\|}\, t$ is the spin distribution parameter, t is thermodynamic temperature, $F_{\|} = 6/\pi^2 < m^2 > (1 - 2/3\varepsilon)$, where $< m^2 >$ is the average value of the squared projection of the angular momentum of the single-particle states, and ε is quadrupole deformation parameter.

For a deformed axially symmetric nucleus

$$K_{rot}(U) = \sigma_{\perp}^2 = F_{\perp}t \tag{7}$$

where $\sigma_{\perp}^2$ is the spin cutoff parameter, $F_{\perp}$ is the nuclear momentum of inertia (perpendicular to the symmetry axis), which equals the rigid-body value at high excitation energies, where the pairing correlations are destroyed. The momentum of inertia takes an experimental value at zero temperature and is interpolated in between, using the pairing model.

For triaxially asymmetric nuclides the rotational enhancement factor is

$$K_{rot}(U) = 2\sqrt{2\pi}\sigma_{\perp}^2\sigma\ . \tag{8}$$

The closed-form expressions for thermodynamic temperature and other relevant equations which one needs to calculate $\rho(U, J, \pi)$ are provided by Ignatyuk et al. [22]

The collective contribution of the level density of deformed nuclei is defined by the nuclear deformation order of symmetry. The actinide nuclei at equilibrium deformation are axially symmetric. We adopted the order of symmetry of nuclear shape at inner and outer saddles from calculations within shell correction method (SCM) by Howard & Möller [23]. The main parameter of the level density a was obtained by fitting the neutron resonance spacing. The neutron resonance spacing $< D_{obs} > = 20.761$ eV and $< D_{obs} >= 2.973$ eV for ^{238}U and ^{237}U target nuclides, respectively, were obtained using a method, which takes into account the correlation of weak resonance missing and resonance missing due to poor experimental resolution [24].

We will illustrate cumulative number of levels description with constant temperature approximation for ^{239}U and ^{238}U nuclides. The cumulative number of observed levels for even-even ^{238}U and even-odd ^{239}U are compared with constant temperature approximation in Figs. 1 and 2. In case of ^{238}U missing of levels above pairing gap is markedly pronounced. In case of ^{239}U nuclide missing seems to be pronounced above excitations of 0.3 MeV

The quasiparticle level density $\rho_{qp}(U, J, \pi)$ is defined as follows:

$$\rho_{qp}(U, J, \pi) = \frac{(2J+1)\omega_{qp}(U)}{4\sqrt{2\pi}\sigma_{\perp}^2\sigma_{\parallel}} \exp\left(-\frac{J(J+1)}{2\sigma_{\perp}^2}\right). \tag{9}$$

Few-quasiparticle effects which are due to pairing correlations are essential for state density calculation at low intrinsic excitation energies either for equilibrium and saddle deformations. The step-like structure in ^{239}Pu(n,2n) reaction cross section was shown to be a consequence of threshold excitation of two-quasiparticle configurations in residual even-even nuclide ^{238}Pu [15]. The same effect is pronounced in ^{238}U(n,γ) data description through (n,γn$'$) reaction competition [25]. We argue that they are important also for reasonable fitting of inelastic scattering cross section data for even-even target nuclide ^{238}U at low energies, typically below $\sim$2 MeV incident neutron energy. In case of even-odd fissioning nuclide ^{239}U few-quasiparticle effects are also important for description of over-threshold irregularities evident in fission cross section data [26].

The partial $n-$quasiparticle state densities, which sum-up to intrinsic state density of quasiparticle excitations could be modelled using the Bose-gas model prescriptions [15, 27].The intrinsic state density of quasiparticle excitations $\omega_{qp}(U)$ could be represented as a sum of $n-$quasiparticle state densities $\omega_{nqp}(U)$:

$$\omega_{qp}(U) = \sum_n \omega_{nqp}(U) = \sum_n \frac{g^n(U-U_n)^{n-1}}{((n/2)!)^2(n-1)!}, \tag{10}$$

where $g = 6a_{cr}/\pi^2$ is a single-particle state density at the Fermi surface, n is the

number of quasiparticles.

The threshold values for excitation of $n-$quasiparticle configurations are calculated from [27]. The partial $n-$quasiparticle state densities $\omega_{nqp}(U)$ depend critically on the threshold values U_n for excitation of the n-quasiparticle configurations, $n = 2, 4...$ for even-even nuclei and $n = 1, 3...$ for odd-A nuclei. The values of U_n could be defined as follows from [27] :

$$U_n = \begin{cases} E_{cond}(3.23n/n_{cr} - 1.57n^2/n_{cr}^2), & \text{if } n < 0.446n_{cr} \\ E_{cond}(1 + 0.627n^2/n_{cr}^2), & \text{if } n \geq 0.446n_{cr}. \end{cases} \tag{11}$$

Here, $n_{cr} = 12/\pi^2(ln2)gt_{cr}$, critical temperature $t_{cr} = 0.571\Delta$, condensation energy $E_{cond} = 0.152a_{cr}\Delta^2 - m\Delta$, with m=0, 1, 2 for even-even, odd-A and odd-odd nuclides, respectively. This U_n value estimate embodies the energy dependence of the correlation function $\Delta(U)$ as well as a modified Pauli correction to the excitation energy. The angular momentum distribution parameter $\sigma_{\|}^2$ could be represented as

$$\sigma_{\|}^2 = \sum_n n\langle m^2\rangle\omega_{nqp}(U)/\sum_n \omega_{nqp}(U), \tag{12}$$

where $\langle m^2\rangle = 0.24A^{2/3}$ is the average value of the squared projection of the angular momentum of the single-particle states on the symmetry axis.

The pairing is weakened by excitation of few-quasiparticle states; virtually only lowest quasiparticle number states (n =2 for even nuclei and n =1 for odd nuclei) lead to pronounced structure in total level density for actinide nuclei [15]. In case of even-even nuclei intrinsic two-quasiparticle state density $\omega_2(U)$ could be represented by an equation, modifying $\omega_2(U) = g^2(U - U_2)$ with a Woods-Saxon expression at excitations below four-quasiparticle excitation threshold:

$$\omega_2(U) = g^2(U_4 - U_2 - \alpha)(1 + exp((U_2 - U + \beta)/\gamma))^{-1}. \tag{13}$$

This estimate of $\omega_2(U)$ was obtained by modelling the structure of ^{238}Pu intrinsic state density to interpret observed step-like structure in ^{239}Pu(n,2n) reaction data near threshold [15]. Here we will model this type of step-like behavior with constant temperature model parameters. We modelled the nuclear level density $\rho(U)$ of even-even nuclei above the pairing gap up to the four-quasiparticle excitation threshold as

$$\rho(U) = \rho(U_4 - \delta_4)/(1 + \exp(U_2 - U + \delta_a)/\delta_s). \tag{14}$$

This estimate almost coincides with that, obtained with Bose-gas modelling of intrinsic state density. The numerical values of δ_4 =0.3 MeV, ($\delta_4 \sim 0.5(U_4 - U_2)$), δ_a =0.1 MeV, δ_s = 0.1 MeV parameters, for residual nucleus, defining shape of $\rho(U)$ are extracted by fitting total inelastic and fission cross section data of ^{238}U. The total level density for even nuclide ^{238}U at equilibrium deformation, calculated with Eqs. (5-14), as compared with the Gilbert-Cameron-type approximation of $\rho(U)$ is shown in Fig. 3. The arrows on the horizontal axis of

Fig. 3 indicate the excitation thresholds of even $n-$quasiparticle configurations. Below the excitation threshold U_2, i.e. within pairing gap the constant temperature model fits cumulative number of ^{238}U levels. Actually the collective levels of ENSDF [28] are employed within pairing gap.

In case of odd-even and even-odd nuclei the partial contributions of $n-$quasiparticle states $\omega_{nqp}(U)$ to the total intrinsic state density $\omega_{qp}(U)$ produces distinct "jump" only below three-quasiparticle excitation threshold U_3 (see Fig. 4). Nuclear level density $\rho(U)$ up to the three-quasiparticle excitation threshold U_3 is virtually independent of the excitation energy, since the intrinsic state density ($\omega_1 \sim g$) is constant. In this excitation energy region we will model the level density as

$$\begin{aligned} \rho(U) &= T_f^{-1}(1 + 2.5(U - 0.5U_3)\exp((U_3 + \Delta_f - U_o - \delta_3)/T_f) \\ &\sim \exp((\Delta_f - U_o)/T_f). \end{aligned} \tag{15}$$

Above the three-quasiparticle states excitation threshold the constant temperature model is used, since the intrinsic state density here is virtually a smooth function of excitation energy. For excitation energies below five-quasiparticle and above three-quasiparticle states excitation threshold the level density could be slightly increased, as compared with constant temperature model approximation:

$$\rho(U) = T_f^{-1}\exp((U - U_o + \delta_5)/T_f). \tag{16}$$

The numerical values of parameters δ_3 =1.2 MeV and $\delta_5 = 0.075$ MeV are defined by fitting ^{238}U fission cross section data.

The shell correction dependence of $a-$parameter is defined using the following equation [22]:

$$a(U) = \begin{cases} \tilde{a}(1+ \delta W f(U - E_{cond})/(U - E_{cond})), & U > U_{cr} = 0.47 a_{cr}\Delta^2 - m\Delta \\ a(U_{cr}) = a_{cr} & U \leq U_{cr} = 0.47 a_{cr}\Delta^2 - m\Delta, \end{cases} \tag{17}$$

here m = 0,1,2 for even-even, odd-A and odd-odd nuclei, respectively; $f(x) = 1 - exp(-\gamma x)$, is the dimensionless function, defining the shell effects dumping; condensation energy $E_{cond} = 0.152 a_{cr}\Delta^2$, where Δ is the correlation function, $\tilde{a}$ is the asymptotic a-parameter value at high excitation energies. We assume that $\tilde{a}$-values for equilibrium and saddle deformations are equal.

The parameters of the level density model for inner and outer saddles and equilibrium deformations are as follows: shell correction δW, pairing correlation functions Δ and Δ_f, at equilibrium deformations Δ =$12/\sqrt{A}$, quadrupole deformation ε and momentum of inertia at zero temperature $F_o/\hbar^2$ are given in Table 1. For ground state deformations the shell corrections were calculated as $\delta W = M^{exp} - M^{MS}$, where M^{MS} denotes liquid drop mass (LDM), calculated with Myers-Swiatecki parameters [29], and M^{exp} is the experimental nuclear mass.

Shell correction values at inner and outer saddle deformations $\delta W_f^{A(B)}$ are adopted following the comprehensive review by Bjornholm and Lynn [30].

Table 1 Level density parameters of fissioning nucleus and residual nucleus

Parameter	inner saddle	outer saddle	neutron channel
δW, MeV	2.5*	0.6	LDM
$\triangle$, MeV	$\triangle_o + \delta^{**}$	$\triangle_o + \delta^{*}$	$\triangle_o$
ε	0.6	0.8	0.24
$F_0/\hbar^2$, MeV^{-1}	100	200	73

*) for axially asymmetric deformations, 1.5 MeV for axially symmetric deformations;

**)$\delta = \Delta_f - \Delta$ value is defined by fitting fission cross section in the plateau region.

3 Optical Potential

Optical potential parameters by Haouat et al. [31] are adopted for n+^{238}U interaction data analysis in previous evaluation of JENDL-3.2 [2], coupling scheme being 0^+-2^+-4^+. Optical potential parameters proposed by Young [32] assume the same coupling scheme and are slightly different from those of Haouat et al. Hence, there would be no direct excitation of 6^+ level of ground state band. We tried optical potential parameter search with 0^+-2^+-4^+-6^+ coupling scheme, using potential parameter values proposed by Young [32] as starting ones. Optical potential parameters were determined by fitting total cross section data, angular distributions and $s-$wave strength function. The following potential parameters were obtained:

$$V_R = 46.29 - 0.3E, MeV, r_R = 1.26\ fm, a_R = 0.63\ fm$$

$$W_D = \begin{cases} 2.92 + 0.4E, MeV, & E \leq 10MeV, r_D = 1.26\ fm, a_D = 0.52\ fm \\ 6.92\ MeV, & E > 10\ MeV \end{cases}$$

$$V_{SO} = 6.2\ MeV, r_{SO} = 1.12\ fm, a_{SO} = 0.47\ fm,$$

3.1 Total Cross Section

Total cross section data fits with present and previous optical potentials [31, 32] are not much different below 10 MeV (see Figs. 5,6). Anyway, the discrepancies are well below the scatter of the measured data points. At incident neutron energies lower than ~0.5 MeV the bulk of the data points is about 0.5 barns lower, than optical model calculations predict. This energy region is important for the first 2^+ level excitation cross section estimation. The measured data

trend was reproduced in JENDL-3.2 evaluation by a χ^2- fit of lower measured data.

Above ~10 MeV the shape of total cross section, calculated with potential by Young [32] is different from our calculation. In the optical potential proposed by Young [32], there is a relatively small volume absorption term. It influences total cross section data fit (see Fig. 7), but changes drastically the reaction cross section shape above ~10 MeV. We argue that adding volume absorption term one faces severe problems with consistent description of fission and (n,xn) reaction cross section data just above 10 MeV incident neutron energy. Elastic cross section data shape is fairly reproduced (see Fig. 8).

3.2 Reaction Cross Section

Figure 9 shows the comparison of reaction cross sections, calculated with different coupled channels optical potentials. It will be shown below that the decreasing trend of reaction cross section above ~10 MeV is very important for consistent measured data description. Reaction cross section shapes, calculated with different optical potentials, appear to be rather different. Below ~0.1 MeV the discrepancies are due to fitting different values of $s-$wave strength functions, value of $S_o = 1.16 \times 10^{-4}(\mathrm{eV})^{-1/2}$ [24] which we fitted being the highest.

3.3 Angular Distributions

Elastic scattering angular distribution fit at 3.4 MeV is shown in Fig. 10. Fits with our and other potentials are slightly discrepant only at large angles. As regards inelastic scattering to 2^+ and 4^+ levels at 3.4 MeV incident neutron energy, our fit appears to be shifted to lower values (see Figs. 11, 12).

Elastic scattering angular distributions at 4.5, 5.0, 5.5, 5.9, 6.5, 7.14, 7.5, 8.03, 8.4, 8.56, 9.06, 9.5, 10, 14.1 MeV are shown in Figs. 13-26. Fits with our potential appear to be somewhat better at 4.5, 5.0, 5.5, 5.9, 6.5, 7.14 MeV incident neutron energies and equally good at 8.03, 8.4, 8.56 MeV as compared with other potentials. At higher energies of 9.06, 9.5, 10, 14.1 MeV scattering data to large angles (above ~90°) are described rather poorly with any potential.

Possibility of improving angular distribution at 14.1 MeV with soft-rotator optical potential model, which gives essentially higher reaction cross section estimate was addressed recently[18]. However, the reaction cross section in that case is ~20% higher than that, calculated with present optical potential model. This high value is inconsistent with other measured data base and cannot be accepted.

4 Fission Cross Section

The fission cross-section data is used as a major constraint for inelastic scattering cross section estimation. Consistent description of measured data at deep subthreshold excitations and in the first 'plateau' might justify the validity of level density description and fission barrier parameterization.

4.1 Fission Channel

Analyzing neutron-induced fission data in a double humped fission barrier model, fission process can be viewed as a two-step process, i.e., successive crossing over the inner hump A and over the outer hump B. Hence, the transmission coefficient of the fission channel $T_f^{J\pi}$ (U) can be represented as

$$T_f^{J\pi}(U) = \frac{T_{fA}^{J\pi}(U)T_{fB}^{J\pi}(U)}{(T_{fA}^{J\pi}(U) + T_{fB}^{J\pi}(U))}. \tag{18}$$

The transmission coefficient $T_{fi}^{J\pi}(U)$ is defined by the level density $\rho_{fi}(\varepsilon, J, \pi)$ of the fissioning nucleus at the inner and outer humps (i = A,B, respectively):

$$T_{fi}^{J\pi}(U) = \sum_{K=-J}^{J} T_{fi}^{JK\pi}(U) + \int_0^U \frac{\rho_{fi}(\epsilon, J, \pi)d\epsilon}{(1 + \exp(2\pi(E_{fi} + \epsilon - U)/h\omega_i))}, \tag{19}$$

where the first term denotes the contribution of low-lying collective states, the second term that from the continuum levels at the saddle deformations, and ϵ is the intrinsic excitation energy of fissioning nucleus. The first term contribution due to discrete transition states is dependent upon saddle symmetry. The total level density $\rho_{fi}(\epsilon, J, \pi)$ of the fissioning nucleus is determined by the order of symmetry of nuclear saddle deformation.

Inner and outer fission barrier heights and curvatures as well as level densities at both saddles are the model parameters. They are defined by fitting fission cross section data at incident neutron energies below emissive fission threshold. Fission barrier height values and saddle order of symmetry are strongly interdependent. The order of symmetry of nuclear shape at saddles was defined by Howard and Möller [23] within shell correction method (SCM) calculation. We adopt the saddle point asymmetries from SCM calculations. These saddle asymmetries depend on Z and N of the fissioning nucleus. According to shell correction method (SCM) calculations of Howard and Möller [23] the inner barrier was assumed axially symmetric in case of U compound systems with $A \leq 236$ and asymmetric for $A > 236$. This helps to interpret the non-threshold fission cross section behavior of ^{232}U(n,f) [47] assuming a lowered height of axially symmetric inner hump of ^{233}U, as anticipated by Howard and Möller [23] with SCM calculations. Outer barrier for uranium nuclei is assumed mass-asymmetric.

4.1.1 Fission Transmission Coefficient, Level Density and Transition State Spectrum

Fission cross section data of ^{238}U exhibits almost classic threshold shape, since vibrational resonance at ~1.15 MeV is rather weak. The different behavior of level densities of even-odd and even-even nuclei at low excitation energies should be taken into account. Adopted level density description allows to fit subthreshold cross section shape (see Fig. 27). Incident neutron energy $E_3 = U_3 + E_{fA(B)} - B_n$ correspondent to excitation of three-quasiparticle states is $\sim$ 3 MeV. The one-quasiparticle neutron states of even-odd fissioning nuclide, lying below the three-quasiparticle states excitation threshold define the shape of fission cross section below incident neutron energy of $E \leq E_{fA(B)} + U_3 - B_n$. At higher excitation energies three-quasiparticle states are excited. Two-quasiparticle states in even residual nuclide ^{238}U could be excited at incident neutron energies $E > U_2$. At lower energies fission cross section shape is controlled by one-quasiparticle state density. The transition state spectra were constructed using values of $F_0/\hbar^2$ at the inner and outer saddles shown in Table 1.

Each one-quasiparticle state in odd fissioning nucleus is assumed to have a rotational band built on it with a rotational constant, dependent upon the respective saddle deformation. We construct the discrete transition spectra up to ~100 keV, using one-quasiparticle states by Bolsterli et al. [48] (see Table 2). The discrete transition spectra, as well as continuous level contribution to the fission transmission coefficient are dependent upon the order of symmetry for fissioning nucleus at inner and outer saddles. Due to the axial asymmetry at the inner saddle we additionally assume $(2J + 1)$ rotational levels for each J value. The negative parity bands $K^\pi = 1/2^-, 3/2^-, 5/2^-$ ... at outer saddle are assumed to be doubly degenerate due to mass asymmetry. With transition state spectra thus defined the fission barrier parameters are obtained. Uranium non-fissile target cross sections are not very sensitive to the discrete level spectra at the lower outer barrier.

Table 2 Transition spectra band-heads Z-even, N-odd nuclei

inner saddle		outer saddle	
K^π	E_{K^π}, MeV	K^π	E_{K^π}, MeV
$1/2^+$	0.0	$1/2^+$	0.0
$5/2^+$	0.08	$1/2^-$	0.0
$1/2^-$	0.05	$3/2^+$	0.08
$3/2^-$	0.0	$3/2^-$	0.08
		$5/2^+$	0.0
		$5/2^-$	0.0

4.2 Fission Data Analysis

Measured data for ^{238}U fission cross section are available in deep subthreshold energy range. Below ~2 MeV incident neutron energy data by Behrens et al. [49], Fursov et al. [50], Meadows et al. [51, 52] and Vorotnikov et al. [53] are compatible (see Fig. 27). At higher incident neutron energies shapes of data by Behrens et al. [49] and Fursov et al. [50] are slightly different. Data by Androsenko et al. [54] exhibit rather large scatter below 3.6 MeV. The most peculiar feature of measured data base is a "cusp" in the energy range of 2 - 4 MeV. We assume it to be due to interplay of level densities of even-odd fissioning nuclide ^{239}U and residual nuclide ^{238}U (see Fig. 28).

One-quasiparticle neutron states of even-odd ^{239}U fissioning nuclide, lying below three-quasiparticle states excitation threshold define the shape of ^{238}U fission cross section below incident neutron energy of ~2.8 MeV. Irregularities at ~1.15 MeV and ~0.4 MeV are attributed to second well vibrational resonances. At higher energies three-quasiparticle states are excited. We fit the data by Fursov et al. [50] with relevant level density parameters.

5 Inelastic Scattering

Main competing channels against inelastic scattering are elastic scattering, capture and fission. Elastic scattering competition is of overwhelming importance below ~2 MeV incident neutron energy. At higher energies fission channel competition is decisive.

5.1 Neutron Channel

The lumped transmission coefficient of the neutron scattering channel is given by

$$T_n^{J\pi}(U) = \sum_{l'j'q} T_{l'j'}^{J\pi}(E - E_{q'}) + \sum_{l'j'I'} \int_0^{U-U_c} T_{l'j'}^{J\pi}(E')\rho(U - E', I', \pi)dE', \qquad (20)$$

where $\rho(U-E', I', \pi)$ is the level density of the residual nucleus. Levels of residual nuclide ^{238}U are provided in Table 3. The entrance channel neutron transmission coefficients $T_{lj}^{J\pi}$ are calculated within a rigid rotator coupled channel approach. For the compound nucleus formation cross section calculation, the cross sections of the direct excitation of ground state band levels were subtracted from the reaction cross section. The compound and direct inelastic scattering components are added incoherently. The coupled channel calculations as well as the statistical model calculations were performed with the computer code STAT [55].

The exit neutron transmission coefficients $T_{l'j'}^{J\pi}(E')$ were calculated using the same deformed optical potential, as that for the entrance channel, but without

coupling. This approximation may lead to some error, however we believe that the influence of the coupling scheme, which is different from that in the entrance channel would not be too large.

Below 5 MeV incident neutron energy, due to high fission threshold the main contribution to inelastic scattering on ^{238}U comes from the compound processes (see Figs. 29-43). For ground state band levels the direct and compound components became comparable above ~1.5-2 MeV. As regards γ-vibration band levels the direct component contribution never exceeds ~10 mbarns.

Table 3 Levels of ^{238}U

E, MeV	J^π	K^π	E, MeV	J^π	K^π
1.0566	4^+	2^+	1.0595	3^+	2^+
1.0373	2^+	0^+	1.0603	2^+	2^+
0.9975	3^-	1^-	1.0765	12^+	0^+
0.993	0^+	0^+	1.1057	3^+	2^+
0.9673	2^+	2^+	1.1126	1^-	1^-
0.9663	7^-	0^-	1.1270	4^+	2^+
0.9502	2^-	1^-	1.1287	2^-	1^-
0.9308	1^-	1^-	1.1503	9^-	0^-
0.9257	0^+	0^+	1.1680	4^+	2^+
0.8267	5^-	0^-	1.1704	3^-	1^-
0.7757	10^+	0^+			
0.7319	3^-	0^-			
0.6801	1^-	0^-			
0.5183	8^+	0^+			
0.3072	6^+	0^+			
0.1484	4^+	0^+			
0.0449	2^+	0^+			
0.0000	0^+	0^+			

5.2 Ground State Rotational Band

The first excited level cross section is the most extensively studied (see Fig. 29), nonetheless the data points scatter a lot below ~0.8 MeV. Calculated cross section shape is controlled by competition of elastic scattering. Calculated cross section value around 0.6 MeV seems to be the highest attainable with present approach. The compound component tends to be zero above ~3 MeV incident neutron energy. The present and previous coupling scheme and potential parameters are somewhat different, so the discrepancies below ~3 MeV are due to both direct and compound contribution estimates. The present calculation

describes essentially the data by Kornilov et al. [56] and Beghian et al. [57]. We increased the cross section around the maximum of the first excited level cross section up to the data by Kornilov et al. [56], indirectly taking them into account while searching optical potential parameters. The calculated cross section of 4^+-level excitation is somewhat different from the previous evaluations below ~1 MeV incident neutron energy (see Fig. 30), although it is compatible with measured data well within data errors. The present 6^+- level excitation cross section is close to evaluation of JENDL-3.2 below 1.4 MeV (see Fig. 31). We employ coupling schema of 0^+-2^+-4^+-6^+, direct contribution of 6^+-level excitation is predominant above ~2 MeV. Direct contribution should be virtually zero, when using coupling basis of 0^+-2^+-4^+. We may conclude, that 6^+- level excitation cross section evaluations of JENDL-3.2 and ENDF/B-VI are not pure calculations, they were normalized to reproduce measured data trend.

The direct excitation cross section of ground state rotational band levels 0^+-2^+-4^+-6^+ changes very smoothly up to 20 MeV.

5.3 Soft Rotator Model

Another direct component is due to excitation of octupole and quadrupole band levels. Direct excitation cross sections for $\gamma(\beta)$-vibration ($K^\pi = 0^+, 2^+$) as well as octupole ($K^\pi = 0^-$) band levels are calculated with a soft rotator model [18]. Actually the calculations were made adding each $K^\pi = 0^+, 2^+, 0^-$ band level one by one to the 0^+-2^+-4^+-6^+ coupling basis, since the coupling with ground state band levels is the strongest for any level (see Table 4). In other words, five levels were coupled.

In a soft rotator model, e.g. deformed non-axial, soft to quadrupole vibrations rotor, collective states structure is described [18], so the coupling strength parameters were derived. The differential scattering data [8] for negative parity level excitations at 1.5 MeV and 2 MeV incident neutron energy are no good to fix reliable values of octupole equilibrium deformation parameter. The reason is very low contribution of direct scattering, as compared with compound one.

5.3.1 Octupole Band

The respective direct component contribution never exceeds ~20 mbarns above 10 MeV [65]. The most pronounced is the direct excitation contribution for the $K^\pi=0^-$ band head state 0.6801 MeV ($J^\pi=1^-$). Evaluated curves are rather consistent, except JEF-2 data (see Fig. 32). The same is the case for second 0.7319 MeV ($J^\pi=3^-$) (see Fig. 33) and third 0.8267 MeV levels ($J^\pi=5^-$) of $K^\pi = 0^-$ band (see Fig. 34). One may assume that the ENDF/B-VI curve only somewhat overestimates this cross section, however this is a kind of systematic overestimation, since in case of third level 0.8267 MeV ($J^\pi=5^-$) of $K^\pi=0^-$ band the discrepancy is much larger (see Fig. 34). The excitation cross section of the

second member 0.9502 MeV ($J^\pi=2^-$) of the octupole band $K^\pi=1^-$ is shown in Fig. 36.

Table 4 Coupling scheme for ^{238}U

				1.1680; 4^+
	1.1503 9^-			
			1.1270 4^+	
				1.1057; 3^+
				1.0603; 2^+
		1.0566; 4^+		
			1.0373; 2^+	
			0.993; 0^+	
		0.9673; 2^+		
	0.9663; 7^-			
		0.9257; 0^+		
	0.8267; 5^-			
	0.7319; 3^-			
	0.6801; 1^-			
0.3072; 6^+				
0.1484; 4^+				
0.0449; 2^+				
0.0000; 0^+				
$K^\pi= 0^+$	$K^\pi= 0^-$	$K^\pi= 0^+$	$K^\pi= 0^+$	$K^\pi= 2^+$

5.3.2 Quadrupole Band

The comparison of combined excitation cross section of γ-vibration band-head 0.9257 MeV ($K^\pi=0^+$) and octupole band-head 0.9308 MeV ($K^\pi=1^-$) with measured data is shown in Fig. 35. Noticeable discrepancy of present calculation and JENDL-3.2 estimate is observed only above ~1.2 MeV. The direct excitation cross section of 0.9257 MeV ($K^\pi=0^+$) level is lower than 10 mbarns. Present calculation almost coincides with JENDL-3.2 estimate above 1.5 MeV.

The excitation cross section of $K^\pi=0^-$ octupole band member 0.9663 MeV ($J^\pi=7^-$) is rather small, so the combined cross section shown in Fig. 37 is essentially that of second member of γ-vibration band $K^\pi=0^+$- 0.9673 MeV ($J^\pi=2^+$), present calculation is consistent with JENDL-3.2 estimate below 1.8 MeV, at higher energies the discrepancy is due to direct excitation of 0.9673 MeV ($J^\pi=2^+$) level.

The comparison of calculated combined excitation cross section of β-vibration band-head 0.993 MeV ($K^\pi=0^+$) and octupole band $K^\pi=1^-$ third member - 0.9975 MeV ($J^\pi=3^-$) with measured data is shown in Fig. 38. The level quoted by Shao

et al. [8], 0.9983 MeV (J^π=2^+), is missing in adopted level scheme of ENSDF [28]. Noticeable discrepancy of present calculation and JENDL-3.2 evaluations with measured data is observed only above ~1.5 MeV. The same kind of calculated curve discrepancy with measured data is observed for second level of β-vibration band K^π=0^+, 1.0373 MeV (J^π=2^+) (see Fig. 39), however increasing data trend at higher energies hardly can be interpreted.

The comparison of calculated combined excitation cross section of γ-vibration bands with K^π=$0^+$and K^π=2^+ levels of 1.0566 MeV (J^π=4^+) and 1.0603 MeV (J^π=2^+), respectively, is shown in Fig. 40. Quoted level at 1.0595 MeV (J^π=3^+) is missing in adopted level scheme. Noticeable discrepancy of present calculation and JENDL-3.2 evaluations with measured data is observed only above ~1.5 MeV. The contribution of direct excitation of 1.0566 MeV (J^π=4^+) and1.0603 MeV (J^π=2^+) levels is shown.

Figure 41 shows the comparison of calculated cross section for second member of γ-vibration band K^π=2^+- 1.1057 MeV (J^π=3^+), present calculation is also consistent with JENDL-3.2 estimate. The same kind of calculated curve discrepancy with measured data is observed as for second level of β-vibration band K^π=0^+, 1.0373 MeV (J^π=2^+), however increasing data trend at higher energies also hardly can be interpreted.

Figure 42 shows the comparison of calculated combined cross section for the third member of β-vibration band K^π=0^+- 1.127 MeV (J^π = 4^+) and second member of octupole band K^π=1^- of 1.1287 MeV (J^π = 2^-). Present calculation also is consistent with JENDL-3.2 estimate.

Figure 43 shows the comparison of combined calculated cross section for third member of γ-vibration band K^π=2^+- 1.168 MeV (J^π=4^+) and second octupole band K^π= 1^- level of 1.1701 MeV (J^π=2^-), present calculation and JENDL-3.2 estimate well coincide with measured data. The contribution of direct excitation of 1.168 MeV (J^π=4^+) level is shown.

5.4 Total Inelastic Cross Section

Calculated total inelastic cross section is compared with measured data in Fig. 44. Measured data seem to be somewhat inconsistent. The data measured by Kornilov et al. [11] and Smith et al. [10] should be complemented with the inelastic scattering cross sections for low-energy levels, falling out of the integration of scattered neutron spectra. The calculated curve describes the measured data base rather well. The contribution of direct excitation of ground state band levels, octupole and γ-vibration levels is shown to be ~20% at most. The step-like dependence of total inelastic scattering cross section above 1.5 MeV incident neutron energy is compatible with measured data base. The decreasing trend of the calculated curve is supported by the data point, measured by Baba et. al. [38] at 6 MeV. The calculated curve is consistent with JENDL-3.2 evaluation around 2 MeV incident neutron energy. Figure 45 shows the comparison of con-

tinuum scattering contribution to total inelastic cross section. Above ~8 MeV continuum scattering cross section goes lower than that of direct level excitation.

Above emissive fission threshold evaluations of inelastic scattering cross section appear to be inconsistent, present estimate being the lowest. The discrepancy with JENDL-3.2 evaluation might be attributed to overestimated contribution of preequilibrium neutron emission in JENDL-3.2 (see Fig. 46). In our calculations preequilibrium neutron emission contribution is defined by description of secondary neutron spectra [68] and ^{238}U(n,2n) reaction cross section [69].

5.5 Evaluated Inelastic Scattering Cross Section of JENDL-3.2

In JENDL-3.2 evaluation [6] direct scattering contribution was included for ground state band and vibrational bands. It is commented that no direct excitation was included for 1.0595 MeV; $J^\pi = 3^+$, 1.1126 MeV; $J^\pi = 1^-$, 1.2242 MeV; $J^\pi = 2^+$ and 1.2785 MeV; $J^\pi = 1^-$ levels. Optical potential by Haouat et al. [31] was used, while β-coupling strengths were defined by fitting data on excitation cross sections for ground state, quadrupole and octupole vibrational bands. Compound inelastic scattering contributions for first and second excited levels were calculated with ECIS[70] code. The other levels excitation cross sections were calculated with Hauser-Feshbach-Moldauer theory. Subsequently, compound contributions of discrete level excitation cross sections, except that of first level, were multiplied by empirical factor of 0.91, to get better agreement with total inelastic scattering data. Besides, hypothetical levels at 1.5, 2.0, 2.5, 3.0, 3.5 and 4.0 were introduced.

6 Capture Cross Section

A source of controversy about capture cross section below ~150 keV incident neutron energy is the discrepancy of integral and differential measurements. It was addressed by NEA Working Group on International Evaluation Cooperation [71] recently. Actually, calculated values of capture-to-fission reaction ratios for fast assemblies are 10 to 15% higher than experimentally determined. It was recommended that evaluated capture cross section should be normalized to the level, expected from the reactor physics analysis. Another difficulty is due to inconsistency between the radiative strength function value implied by $s-$wave radiation width and neutron resonance spacing ($\langle\Gamma_\gamma\rangle$ = 23.6 meV, $\langle D_{obs}\rangle$ = 21.5 eV, as quoted by Fröhner [72]) and the average resonance cross sections fitted in the region of ~10 to 300 keV [72]. Difference amounts to ~9% and could be removed by spin and parity reassignments of weak resonances [72], which might lead to ~10% increase of $\langle D_{obs}\rangle$ estimate. Our estimates of relevant average resonance parameters are as follows: $\langle\Gamma_\gamma\rangle$ = 23.6±0.8 meV, $\langle D_{obs}\rangle$ = 20.761±0.3

eV. They are consistent with RIPL [73] recommendations and increase of $\langle D_{obs} \rangle$ estimate is doubtful. However, we may feel free to vary radiative strength function value to fit recommended [71] measured capture data.

6.1 Radiative Capture Channel

Estimates of ^{238}U capture cross section are much dependent upon radiative strength function value. Radiative strength function value is defined by radiative capture width and neutron resonance spacing of ^{238}U. The dipole radiative strength function was calculated using Lorenzian parameterization of actinide absorption cross section data at low energies (<7 MeV). The higher multipolarity transitions are neglected. The radiative transmission coefficient

$$T_{\gamma}^{J\pi}(U) = \frac{2\pi C_{\gamma}}{3(\pi hc)^2} \int \varepsilon_{\gamma}^2 \sigma_{\gamma}(\varepsilon_{\gamma}) \sum_{I=|J-1|}^{I=J+1} \rho(U - \varepsilon_{\gamma}, I, \pi) d\varepsilon_{\gamma}, \tag{21}$$

was calculated using Lorenz' parameterization of photoabsorption cross section $\sigma_{\gamma}(\varepsilon_{\gamma})$

$$\sigma_{\gamma}(\varepsilon_{\gamma}) = \sum_{i=1}^{2} \sigma_{\gamma i} \frac{\varepsilon_{\gamma}^2 \Gamma_{Gi}^2}{(\varepsilon_{\gamma}^2 - E_{Gi}^2)^2 + \varepsilon_{\gamma}^2 \Gamma_{Gi}^2}. \tag{22}$$

The respective parameters being fitted to actinide photoabsorption data at low energies [74] are as follows: $\sigma_{\gamma 1} = 250\ mb$, $\sigma_{\gamma 2} = 300\ mb$, $E_{G1} = 10.5\ MeV$, $E_{G2} = 14\ MeV$, $\Gamma_{G1} = 2.5\ MeV$, $\Gamma_{G2} = 4.5\ MeV$, C_{γ} is the normalizing coefficient.

At incident neutron energies higher than ~1 MeV, the competition of neutron emission at the second cascade, i.e. after first γ-quanta emission should be included. Then "true" capture reaction cross section $(n, \gamma\gamma)$ is defined using transmission coefficient $T_{\gamma\gamma}^{J\pi}(U)$ given in a two-cascade approximation as

$$T_{\gamma\gamma}^{J\pi} = \frac{2\pi C_{\gamma 1}}{3(\pi hc)^2} \int \varepsilon_{\gamma}^2 \sigma_{\gamma}(\varepsilon_{\gamma}) \sum_{I=|J-1|}^{I=J+1} \rho(U - \varepsilon_{\gamma}, I, \pi) \frac{T_{\gamma}^{I\pi}}{T_f^{I\pi} + T_{n'}^{I\pi} + T_{\gamma}^{I\pi}} d\varepsilon_{\gamma}\ , \tag{23}$$

The last term of the integrand describes the competition of fission, neutron emission and γ-emission at excitation energy $(U - \varepsilon_{\gamma})$ after emission of first γ-quanta, $C_{\gamma 1}$ is the normalizing coefficient. That means transmission coefficients $T_{\gamma}^{I\pi}$, $T_{n'}^{I\pi}$ and $T_f^{I\pi}$ are defined at excitation energy $(U - \varepsilon_{\gamma})$. The neutron emission after emission of first γ−quanta strongly depends on the ^{238}U residual nuclide level density at excitations just above paring gap [25].

The contribution of $(n, \gamma n')$−reaction to inelastic scattering cross section is defined by $T_{\gamma n'}^{J\pi}$ value. The energy dependence of $(n, \gamma n')$ reaction transmission coefficient $T_{\gamma n'}^{J\pi}$ was calculated with the expression

$$T_{\gamma n'}^{J\pi} = \frac{2\pi C_{\gamma 1}}{3(\pi hc)^2} \int \varepsilon_\gamma^2 \sigma_\gamma(\varepsilon_\gamma) \sum_{I=|J-1|}^{I=J+1} \rho(U-\varepsilon_\gamma, I, \pi) \frac{T_{n'}^{I\pi}}{T_f^{I\pi} + T_{n'}^{I\pi} + T_\gamma^{I\pi}} d\varepsilon_\gamma \ , \quad (24)$$

At incident neutron energies above fission threshold competition of fission is important [75]. The contribution of $(n, \gamma f)$−reaction to fission cross section is defined by $T_{\gamma f}^{J\pi}$ value. The energy dependence of $(n, \gamma f)$ reaction transmission coefficient $T_{\gamma f}^{J\pi}$ was calculated with the expression

$$T_{\gamma f}^{J\pi} = \frac{2\pi C_{\gamma 1}}{3(\pi hc)^2} \int \varepsilon_\gamma^2 \sigma_\gamma(\varepsilon_\gamma) \sum_{I=|J-1|}^{I=J+1} \rho(U-\varepsilon_\gamma, I, \pi) \frac{T_f^{I\pi}}{T_f^{I\pi} + T_{n'}^{I\pi} + T_\gamma^{I\pi}} d\varepsilon_\gamma \ , \quad (25)$$

The capture data description is shown in Fig. 47. The $(n, \gamma n')$ reaction competition to the "true" capture $(n, \gamma\gamma)$ reaction competition is rather strong above ~2 MeV incident neutron energy.

6.2 Data Analysis

Capture data status was reviewed by Pönitz et al. [76] about fifteen years ago. Uncertainty of capture cross section data was estimated to be ~5% between 10 and 500 keV and ~10% at 1 MeV. The problem of high cross section data by DeSaussure et al. was addressed, which was subsequently resolved by Moxon (see [71]). It was stressed that ~30% of FBR sensitivity to capture cross section of ^{238}U lies below ~10 keV.

Here is enclosed a short review of selected capture cross section measurements, which reflect major data trends. Capture cross section was measured by Pönitz et al. [77] with the activation technique from 30 keV up to 3 MeV, ^{235}U(n,f) (at higher energies mostly) and ^{197}Au(n,γ) were used as a reference cross section. The results are consistent with those obtained with prompt detection technique by Pönitz et al. [78], relative to ^{197}Au(n,γ). Capture cross section was measured by Pönitz et al. [77] with the prompt γ-rays detection by large liquid scintillator from 20 keV up to 1.2 MeV, ^{197}Au(n,γ) was used as a reference cross section.

Capture cross section data by Kazakov et al. [80] was measured between 4 and 460 keV, relative to ^{7}Li(n,t) and ^{10}B(n,α) cross sections; "black resonance" calibration at 6.67 eV resonance was employed. Data by Kazakov et al.[80] are almost consistent with NEA Working Group[71] recommendations.

We adopt here the following procedure of measured data description. Data by Kazakov et al. [80] up to ~100 keV would be fitted. For this, radiative capture strength function should be decreased as compared with RIPL [73] recommended value. Actually, that corresponds to $\langle \Gamma_\gamma \rangle$ = 20 meV, since $\langle D_{obs} \rangle$ = 20.761 eV. Another option of capture data description is that of using $\langle \Gamma_\gamma \rangle$ = 23.6 meV and $\langle D_{obs} \rangle$ = 20.761 eV. In that case calculated curve would follow the upper

measured data points. The former estimate of radiative capture strength function $S_{\gamma o}$ corresponds to estimate of $S_{\gamma o}$ by Fröhner [72].

Fröhner [72] obtained a simultaneous fit to total, capture and inelastic scattering cross section data in the region of overlapping resonances (10-300 keV). Systematic difference of radiative strength function, extracted from resolved resonances and by average cross section description was exemplified. Fits to average cross section data resulted in $s-$wave radiative strength function, which is $\sim$9 % lower than implied by $S_o = 1.15 \pm 0.12$, $\Gamma_\gamma = 23.5$ meV and $\langle D_{obs} \rangle = 21.5$ eV, $s-$, $p-$, $d-$ and $f-$waves being included. In our calculation $\Gamma_\gamma = 23.6$ meV and $\langle D_{obs} \rangle = 20.761$ eV, to fit average cross sections we also need to decrease $s-$wave radiative strength function, as if $\Gamma_\gamma = 20.0$ meV. Estimate of $\langle D_{obs} \rangle$, with account of missing levels and unresolved multiplets, inconsistency mentioned above could be almost removed, as claimed by Fröhner, by refining spin and parity assignment of weak resonances. Indirect evidence is obtained by Fröhner, when only resonances with >99% $s-$wave probability are included. We assume that this latter procedure is not fully justified.

The important peculiarities of the calculated capture cross section is the cusp above first excited level threshold of $\sim$44 keV up to $\sim$700 keV, another one is cross section drop from $\sim$700 keV up to $\sim$1 MeV (see Fig. 47). The latter drop might be correlated with strong increase of inelastic scattering competition due to increase of residual nuclide ^{238}U number of levels (see Fig. 1). It is evident also in Fig. 44, showing total inelastic scattering cross section. Above $\sim$1 MeV capture cross section is defined mainly by $(n, \gamma n')$ reaction competition. Competition of $(n, \gamma f)$ reaction is almost insignificant, since fission threshold of ^{239}U compound nuclide is rather high.

Evaluation of JENDL-3.2 follows data by Kazakov et al. [80] up to 150 keV, while at higher energies it follows data by Fricke et al. [81].

7 Cross Sections above Emissive Fission Threshold

At higher incident neutron energies when fission reaction of ^{238}U, ^{237}U or ^{236}U compound nuclides is possible after emission of 1, 2 or 3 neutrons, the observed fission cross section is a superposition of non-emissive or first chance fission of ^{239}U and xth-chance fission contributions. These contributions are weighted with a probability of x neutrons emission before fission. For fixed statistical model parameters of residual nuclei ^{238}U, ^{237}U or ^{236}U, fissioning in (n, nf), $(n, 2nf)$ or $(n, 3nf)$ reactions, the behavior of the first-chance fission cross section σ_{f1} should make it possible to reproduce the measured fission cross section σ_f of ^{238}U. A consistent description of a most complete set of measured data on the (n, f), $(n, 2n)$, $(n, 3n)$ and $(n, 4n)$ reaction cross sections for the ^{238}U target nuclide up

to 20 MeV enables one to consider the estimates of σ_{f1} and fission probability $P_{f1}$of the initial compound nuclei ^{239}U as fairly realistic.

Fission cross section of ^{238}U, shown in Fig. 48 demonstrates a step-like structure, relevant to contribution of (n,xnf) reactions to total fission cross sections for $x = 1, 2, 3$. Contribution of first-chance fission appears to be sensitive to level density of residual nuclide ^{238}U. Contribution of second- chance fission of ^{238}U compound nuclide is sensitive to level density of fissioning nuclide ^{238}U. Level density parameter of fissioning nuclide ^{238}U $\tilde{a}$ (Eq. 17) was obtained assuming that it equals $\tilde{a}$ value of ^{238}U compound nuclide at stable deformations. We used an estimate of ^{237}U $\langle D_{obs} \rangle = 2.973 \pm 0.416$ eV, obtained by analysis of resolved resonance parameters [24], which is consistent with preequilibrium contribution into first neutron spectrum [68, 89] and subsequent sharing of $\sigma_r = \sigma_{n,f1} + \sigma_{n,nx}$ reaction cross section into first-chance fission and neutron emission cross sections. To get a consistent fit of measured cross sections up to 20 MeV we decreased $\tilde{a}_f$ of fissioning nuclide ^{238}U by 10%. Cross section of ^{237}U(n,f) reaction is shown in Fig. 49, and it corresponds to (n,nf) fission contribution to measured fission cross section ^{238}U(n,f) (see Fig. 48). We have not tried to reproduce measured bomb-shot data by McNally et al. [90] on ^{237}U(n,f) reaction, because they rise drastically above ~100 keV. Contributions of (n,2nf) and (n,3nf) reactions correspond to neutron-induced fission cross sections of ^{236}U and ^{235}U. Neutron-induced fission cross section of ^{236}U is shown in Fig. 50. Evaluated fission cross section of JENDL-3.2 [2] steeply increases above ~18 MeV, it seems to be incompatible with $(n, 3nf)$ fission reaction contribution to the observed fission cross section (see Fig. 48).

7.1 Shell Effects in First Chance Fission Cross Section

The behavior of the first-chance fission cross section σ_{f1} is obviously related with the energy dependence of the first-chance fission probability of the $A + 1$ nucleus P_{f1}:

$$\sigma_{f1} = \sigma_r(1 - q(E))P_{f1}. \tag{26}$$

Once the contribution of first neutron pre-equilibrium emission $q(E)$ is fixed, the first-chance fission probability P_{f1} of the ^{239}U compound nuclide depends only on the level density parameters of fissioning and residual nuclei. That is, actually it depends on the ratio of shell correction values $\delta W_{fA(B)}$ and δW_n. The results of different theoretical calculations of the shell corrections as well as of the fission barriers vary by $1 \sim 2\ MeV$. The same is true for the experimental shell corrections, which are obtained with a smooth component of potential energy calculated according to the liquid-drop or droplet model. However the isotopic changes of $\delta W_{fA(B)}$ and δW_n [30] are such that P_{f1} viewed as a function of the difference $(\delta W_{fA(B)} - \delta W_n)$ is virtually independent of the choice of smooth

component of potential energy. In addition, existing calculations of the shell corrections do not allow for the influence of the asymmetric deformations on the smooth component of potential energy. Therefore, we shall consider the adopted $\delta W_{fA(B)}$ estimates (see Table 1) to be effective, provided that δW_n are obtained with the liquid drop model. The trend of the first-chance fission cross section σ_{f1} shown in Fig. 48 could be treated as a manifestation of the shell effects in first-chance fission probability. So it can be stated that we have obtained effective estimate of σ_{f1} which corresponds to consistent fit of $(n, 2n)$, $(n, 3n)$ and $(n, 4n)$ reaction cross section data.

7.2 Secondary Neutron Spectra

The hard component of neutron scattering spectra and high energy tail of ^{238}U$(n, 2n)$ reaction cross section are interpreted as being due to the pre-equilibrium evaporation of neutrons [68, 69, 89]. This feature is parameterized within a conventional exciton model, used in STAPRE [17] code. By fitting the measured spectra [91] for $E_n = 6 - 14.7\ MeV$ we get the main parameter of the exciton model, that is the matrix element $M^2 = 10/A^3$. Note that, when calculating the exciton state density, the odd-even back-shift is introduced: $\hat{U} = U - \Delta(2 - n)$. The charge conservation and transition rates renormalization were also employed. With all that in mind and in the STAPRE code [17] a pre-equilibrium emission fraction $q(E)$ leading to depletion of compound nucleus states population is obtained, which approaches $\sim$0.45 at $E_n = 20$ MeV. Largely by diminishing the odd-even dependence of $q(E)$ we can fit the ^{235}U fission data with the same M^2 value. These reasonable model fits give rather strong grounds to consider the estimate of contribution of first neutron pre-equilibrium emission $q(E)$ as fairly realistic. They were used also for interpreting the experimental evidence of pre-equilibrium neutron emission prior to neutron-induced fission of ^{238}U, induced by 14.7 MeV neutrons [89].

7.2.1 Model Calculations of (n,nx) Reaction Spectra

To calculate neutron energy distributions of (n,xnγ) and (n,xnf), x = 1, 2, 3 reactions we use a simple Weisscopf-Ewing evaporation model [68] taking into account fission and gamma emission competition to neutron emission. The pre-equilibrium emission of first neutron is included. First neutron spectra for the (n,nx) reaction is the sum of evaporated and pre-equilibrium emitted neutron contributions. Second and third neutron spectra are assumed to be evaporative. Figures 51 and 52 show the comparison of recent secondary neutron spectra measurements by Baba et al. [92] with present calculations [93]. For incident neutron energy of 14 MeV emissive neutron spectrum is deconvoluted, components of 1st, 2nd and 3d neutron spectra are shown. Flattening of secondary neutron spectrum of 14 MeV in the vicinity of elastic peak and "bump" in case of 6 MeV spectrum

are supposed to be due to direct scattering on quadrupole and octupole band levels. However, in case of 14 MeV spectrum levels of higher lying bands should be included [94].

We have calculated 1st, 2nd and 3d neutron spectra for the (n,nγ), (n,2n) and (n,3n) reactions where applicable. According to the ENDF-6 format the secondary neutron spectra are included in the following way. Calculated spectra were summed up and tabular spectra for the (n,nγ), (n,2n) and (n,3n) reactions were obtained. To clarify the competition of neutron, γ-emission and fission in case of (n,nx) and (n,2nx) reactions the following presentation of spectra is provided.

Figure 53 shows the spectrum of 1st neutron of the reaction (n,nx) and its partial contributions for (n,nγ), (n,2n), (n,nf) (n,2nf) and (n,3n) reactions at incident neutron energy of 14 MeV. Above $\sim$5.5 MeV energy of first emitted neutron, neutron spectrum is of pre-equilibrium nature. Spectrum of (n,nγ) reaction actually is just hard energy tail of pre-equilibrium component of first neutron spectrum. Spectrum of first neutron of (n,2n) reaction is much softer, although pre-equilibrium component still comprise major part of it. First neutron spectrum of (n,3n) reaction is actually of evaporative nature. First neutron spectrum of (n,nf) reaction has rather long pre-equilibrium high-energy tail with a peculiar spike around 8 MeV. First neutron spectrum of (n,2nf) reaction, as that of (n,3n) reaction, is of evaporative nature. Figure 54 compares neutron spectra (n,nγ) reaction of JENDL-3.2, ENDF/B-VI and JEF-2 with present calculation. Neutron spectra of JEF-2 is evaporative, while that of JENDL-3.2 contains also rather weak pre-equilibrium component. Average energies of first neutron spectra for JENDL-3.2 and JEF-2 are different, the former being shifted to higher energies (see Table 5), although it is still lower than that of present evaluation. On the contrary, spectra of ENDF/B-VI and present evaluation have very close average energies (see Table 5), while the shapes are rather different. Note that present calculated spectra are fitted to measured neutron emission spectra data as well as (n,2n), (n,3n) and (n,f) reaction cross sections. Figures 55 and 56 show comparison of neutron spectra for (n,nγ) reaction of JENDL-3.2, ENDF/B-VI and JEF-2 with present calculation at 8 MeV and 6 MeV. Almost the same arguments could be applied as in case of 14 MeV incident neutron energy.

Figure 57 shows the spectrum of 2nd neutron of the reaction (n,2nx) and its partial contributions for (n,2n), (n,3n) and (n,2nf) reactions. Spectrum of (n,2n) neutron seems to be hardest one, it's average energy being $\sim$20% higher than those of (n,3n) and (n,2nf) reactions (see also Table 5). Figure 58 shows the comparison of (n,2n) reaction spectra of JENDL-3.2 and present evaluation at 14 MeV. The discrepancy above $\sim$3 MeV is due to first neutron spectra of (n,2n) reaction (see Fig. 53) being of pre-equilibrium nature. In JENDL-3.2 spectrum of (n,2n) reaction is evaporative. Figure 59 shows the comparison of (n,2n) reaction spectra of JENDL-3.2 and present evaluation at 8 MeV. In contrast to previous figure, present spectrum seems to be softer than that of

JENDL-3.2. The same happens with spectrum of (n,3n) reaction shown in Fig. 60. The partial neutron spectra shown in Figs. 53, 55, 56, 57 are normalized to the contributions of appropriate cross sections to the (n,nx) and (n,2nx) reaction cross sections, respectively.

Table 5. Average energies of secondary neutron spectra

E_n, MeV	1st neutron average energy, MeV									
	(n,n')				(n,2n)		(n,n'f)	(n,3n)		(n,2n'f)
	Pres.	B-VI	J-3.2	JEF-2	Pres.	J-3.2	Pres.	Pres.	J-3.2	Present
3.0	0.62	0.29	0.64	0.59			0.17			
8.0	3.10	2.85	1.57	0.90	0.84	0.81	1.01			0.24
14.0	9.45	9.24	2.97	1.25	3.63	1.37	2.31	1.05	1.14	1.06
20.0	15.4	15.2	4.63	1.51	10.2	1.66	3.65	2.80	1.65	2.65

E_n, MeV	2nd neutron average energy,MeV				
	(n,2n)		(n,3n)		(n,2n'f)
	Present	J-3.2	Present	J-3.2	Present
8.0	0.30	0.63			0.19
14.0	0.94	0.94	0.76	0.90	0.74
20.0	0.79	1.31	1.19	1.31	1.19

E_n, MeV	3d neutron average energy,MeV	
	(n,3n)	
	Present	J-3.2
14.0	0.27	0.66
20.0	0.79	0.84

In summary, inclusion of pre-equilibrium emission changes significantly the average energies of emitted neutron spectra. That is shown in Table 5, where the average secondary neutron energies for current, ENDFB-VI and JENDL-3.2 evaluations are compared. The most significant is the change of neutron spectra of (n,nγ) reaction. First neutron spectra of (n, n'f) reaction also becomes harder, that influences prompt fission neutron spectra. On the other hand, the spectra of 2nd and 3d neutrons become softer.

7.3 (n,xn) Reaction Cross Sections

Estimates of (n,2n), (n,3n) and (n,4n) reaction cross sections for ^{238}U are presented in Figs. 61, 62 and 63. In JENDL-3.2 (n,2n) reaction cross section is a χ^2- fit of measured data by Frehaut et al. [96], Veeser et al. [101], Karius et al. [100]. Noticeable discrepancy is observed between data by Kornilov et al. [98, 99] and Frehaut et al. [96] in the range of 8-12 MeV. Kornilov et al. [98, 99] measured

^{238}U(n,2n) reaction cross section by activation technique. Activity of ^{237}U was defined by 208-keV γ-quanta detected with GeLi-scintillator. ^{238}U(n,f) reaction was used as a flux monitor. Frehaut et al. [96] have measured ^{238}U(n,2n) reaction cross section a large liquid scintillator, to count emitted neutrons directly. The results obtained by Frehaut et al. [97] in another experiment are in agreement with their previous measurements. Data by Frehaut et al. [96] shown in Fig. 61, are taken from the EXFOR data base (entry 20416.021) and are much lower than numerical data, given in original paper [97]. Data by Frehaut et al. [96] were updated by Kornilov et al. [98, 99] using ^{238}U(n,f) reference cross sections of ENDF/B-IV, after that they seem to be consistent with measured data by Kornilov et al. [11]. Shape of calculated cross section, especially it's high-energy tail, is strongly correlated with secondary neutron shape.

Cross section of (n,3n) reaction is less sensitive to pre-equilibrium neutron emission contribution. Calculated curve, shown in Fig. 62 is just the result of fitting fission and (n,2n) reaction cross sections. Evaluated (n,3n) reaction cross section of JENDL-3.2 was normalized to reaction cross section, after (n,f), (n,2n), (n,γ) and (n,n') reaction cross sections were independently evaluated.

Cross section of (n,4n) reaction is shown in Fig. 63 up to 40 MeV incident neutron energy. It was obtained by fitting fission cross section data of ^{238}U by Lisowski et al. [88] in statistical model approach [105].

8 Conclusions

The statistical Hauser-Feshbach-Moldauer model calculation of neutron-induced reaction cross sections for ^{238}U target nucleus shows the fair description of available data base on fission, capture, inelastic scattering. Statistical Hauser-Feshbach model was employed for describing fission, (n,2n), (n,3n) and (n,4n) reaction cross sections. The rigid rotator coupled channel model with present potential parameters gives fair description of inelastic scattering data up to $\sim$6 MeV incident neutron energy. The sophistication of the level density model, as compared with various options of Fermi-gas closed-form expressions, although it still remains rather crude, seems to be unavoidable, since it is supported by a lot of experimental data.

The transparent statistical model approach gives fair description of the measured data base. It seems that the potential of the statistical theory to improve the quality of the inelastic scattering evaluation could be considered almost exhausted. At the current state-of-the-art, analyzing of integral experimental data might be more important. However the present results might be the basis of new evaluation.

Acknowledgements

This work was started within Project B-03 "Actinide Nuclear Data Evaluation" of International Science and Technology Center (Moscow, Russia) and completed during the stay of one of the authors (V.M. Maslov) at JAERI under the framework of the Foreign Scientists Invitation Program of JAERI. Partial support of International Atomic Energy Agency (Vienna, Austria) under Research Contract 8832 is acknowledged by one of the authors (V. Maslov).

The authors wish to thank members of Working Party on International Evaluation Cooperation and Working Party on Measurement Activities of Nuclear Energy Agency Nuclear Science Committee for helpful discussions.

References

[1] Akie H., H. Takano, Proc. Int. Conf. on the Physics of Reactors, Mito, Ibaraki, Japan, September, 16-20, 1996, vol. 3, p. F72, 1996.

[2] JAERI-Data/Code, 98-006 (Part II), (Eds.) K. Shibata and T. Narita, 1998.

[3] Roussin R.W., Young P.G., McKnight R., Proc. Int. Conf. Nuclear Data for Science and Technology, Gatlinburg, USA, May 9-13, 1994, p. 692, J.K. Dickens (Ed.), ANS, 1994.

[4] Blokhin A.V., Fursov B.I., Ignatyuk A.V. et al., Proc. Int. Conf. Nuclear Data for Science and Technology, Gatlinburg, USA, May 9-13, 1994, p. 680, J.K. Dickens (Ed.), ANS, 1994.

[5] Nordborg C., Salvatores M., Proc. Int. Conf. Nuclear Data for Science and Technology, Gatlinburg, USA, May 9-13, 1994, p. 680, J.K. Dickens (Ed.), ANS, 1994.

[6] T. Kawano, N. Fujikawa, Y. Kanda, Proc. of the 1993 Symposium on Nuclear Data, November 18-19, 1993, Tokai, Japan, INDC(JPN)-169/L, JAERI-M 94-019, 1994.

[7] Y. Kanda, N. Fujikawa, T. Kawano, JAERI-M 93-205, 1993.

[8] Shao J. Q., Couchell G.P., Egan J.J., et al., Nucl. Sci. Eng., 92, 350 (1986).

[9] Olsen D.K., Morgan G.L. and McConnel J.W., Proc. Int. Conf. Nuclear Data for Science and Technology, Knoxville, USA, September 6-10, 1980, p. 39, J.L. Fowler, C.H. Johnson, and C.D. Bowman, Eds., NBS (1980).

[10] Smith A.B., Guenter P.T., McKnight R.D., Proc. Int. Conf. Nuclear Data for Science and Technology, Antwerpen, Belgium, September 6-10, 1982, p. 39, K.H. Böckhoff, Ed., Holland (1982).

[11] Kornilov N.V., Kagalenko A.B., Nucl. Sci. Eng., 120, 55 (1995).

[12] Baba M. et al., J. Nucl. Sci. Technol. 27, 7, 601 (1990).

[13] Dossing T., Khoo T.I., Lauritsen T. et al., Phys. Rev. Lett., 75, 1276 (1995).

[14] Khitrov V.A., Sukhovoj A.M., Voinov A.V., IV International Seminar on Interaction of Neutrons with Nuclei, Dubna, Russia, April 27-30, 1996, p. 45, 1996.

[15] Maslov V.M. Zeit. Phys. A, Hadrons & Nuclei, 347, 211 (1994).

[16] Tepel J.W., Hoffman H.M., Weidenmuller H.A. Phys. Lett. 49, 1 (1974).

[17] Uhl M., Strohmaier B., IRK-76/01, IRK, Vienna (1976).

[18] Porodzinskij Yu.V., Sukhovitskij E.Sh, Yadernaya Fyzika, 59, 247 (1996).

[19] Ignatjuk A.V., Maslov V.M., Proc. Int. Symp. Nuclear Data Evaluation Methodology, Brookhaven,USA, October 12-16, 1992, p.440, World Scientific, 1993.

[20] Maslov V.M., Kikuchi Y., JAERI-Research 96-030, 1996.

[21] Moldauer P.A., Phys. Rev., C11, 426 (1975).

[22] Ignatjuk A.V., Istekov K.K., Smirenkin G.N. Sov. J. Nucl. Phys. 29, 450 (1979).

[23] Howard W.M., Möller P. Atomic Data and Nuclear Data Tables, 25, 219 (1980)

[24] Porodzinskij Yu.V., Sukhovitskij E.Sh., Maslov V.M., Proc. Int. Conf. Nucl. Data for Sci. and Technology, Trieste, Italy, May 19-23, 1997, p. 937.

[25] Maslov V.M., Proc. Ninth Int. Symp. Capture Gamma-Ray Spectroscopy and Related Topics, Budapest, Hungary, October 8-12, 1996.

[26] Maslov V.M. Proc. Int. Conf. Nucl. Data for Sci. and Technology, Trieste, Italy, May 19-23, 1997, p.1320.

[27] Fu C. Nucl. Sci. Engng. 86, 344 (1984).

[28] Shurshikov E.N., Nucl. Data Sheets, 53, 601 (1988).

[29] Myers W.O., Swiatecky W.J., Ark. Fyzik, 36, 243 (1967).

[30] Bjornholm S., Lynn J.E. Rev. Mod. Phys., 52, 725 (1980).

[31] Haouat, Lachkar J., Lagrange Ch., et al., Nucl.Sci. Engng. 81, 491 (1982).

[32] Young P.G., INDC(NDS)-335, p.109 (1994).

[33] Hayes S.H., Stoler P., Clement J.M., Goulding G.A., Nucl. Sci. Eng., 50, 243 (1973).

[34] Foster Jr. D.G., Glasgow D.W., Phys. Rev. C, 3, 576 (1971).

[35] Schwartz R.B., Schrack R.A., Heaton H.T., Nucl. Sci. Eng., 54, 322 (1974).

[36] Batchelor R., Gilboy W.B., Towle J.H., Nucl. Phys., 65, 236 (1965).

[37] Uttley C.A., Newstead C.M. and Diment K.M., Proc. Int. Conf. Nuclear Data for Reactors, Paris, France, October 17-21, 1966, vol. 1, p.165, IAEA (1966).

[38] Baba M., Nomoto K., Kanda K., et al. EANDC(J)-30, 66 (1973).

[39] Cabe J., Cance M., CEA-R-4524 (1973).

[40] Poenitz W.P., Nucl. Sci. Eng., 57, 300 (1975), Poenitz W.P., Whalen J.P., Smith A.B., Nucl. Sci. Eng., 78, 333 (1981).

[41] Tsubone I, Nakajima Y., Furuta Y., Kanda Y., Nucl. Sci. Eng., 88, 579 (1984).

[42] Allen R.C., Walton R.B., Perkins R.B., Olson R.A., Taschek R.F., Phys. Rev., 104, 731 (1956).

[43] Barnard E., Ferguson A.T.G., McMurray W.R., Vanheerden I.J, Nucl. Phys., 80, 46 (1966).

[44] Li Jingde, Xie Daquan, Ma Gonggui et al., 86Harrog, 1, 229 (1986).

[45] Shen Guanran, Cao Zhong, Wang Hui-Zhu et al., 81Grenob, 512 (1981).

[46] Voignier J., CEA-3503, 1968.

[47] Maslov V.N., Kikuchi Y., Nucl. Sci. Eng., 124, 492 (1996).

[48] Bolsterli M., Fiset E.O., Nix J.R., Norton J.L. Phys.Rev., C 5, 1050 (1972).

[49] Behrens J.W. and Carlson G.W., Nucl. Sci.Eng., 63, 250 (1977).

[50] Fursov B.I., et al., Sov. J. At. Energy, 43, 808 (1978)

[51] Meadows J.W., Nucl. Sci.Eng., 58, 255 (1975).

[52] Meadows J.W., Nucl. Sci.Eng., 49, 310 (1972).

[53] Vorotnikov P.E., Dubrovina S.M., Otroshchenko G.A., et al., Yaderno-Physycheskie Issledovaniya, 12, 22 (1971).

[54] Androsenko Kh.D., Korolev G.G., Shpak D.L., Neutron Physics, Proc. All-Union Conference, Vol. 2, p.153, Tsniiatominform, Moscow (1983) [in Russian].

[55] Maslov V.M, Porodzinskij Yu.V., Sukhovitskij E.Sh., Proc. Int. Conf. Nucl. Data for Sci. and Technology, Trieste, Italy, May 19-23, 1997, p. 1332.

[56] N.V. Kornilov, A.B. Kagalenko, Proc. IV International Seminar on Interaction of Neutrons with Nuclei, Dubna, Russia, April 27-30, 1996, p. 53, 1996.

[57] Beghian L.E., Kegel G.H.R., Marcella T.V. et al., Nucl. Sci.Eng., 91, 428 (1985).

[58] Guenter P., Havel D., Smith A.B., ANL-NDM-16, 1975.

[59] Tsang F.Y., Brugger R.M., Nucl. Sci. Eng. 65, 70 (1978).

[60] Winters R.R., Hill N.W., Macklin R.L., et al., Nucl. Sci. Eng. 78, 147 (1981).

[61] Strömberg L.G., Schwarz S., Nucl. Phys., 71, 511 (1965).

[62] Murzin A.V., Vertebnij V.P., Kiriljuk A.L. et al., At. Energy, 62, 192 (1987).

[63] Litvinskij L.L., Murzin A.V., Novoselov G.M. et al., Yad. Phys., 52, 1025 (1990).

[64] Vorotnikov P.E., Vukolov V.A., Koltypin E.A, et al., Neutron Physics, Proc. All-Union Conference, Vol. 2, p.119, Tsniiatominform, Moscow (1977) [in Russian].

[65] Porodzinskij Yu.V., private communication.

[66] Kazjula B.G., Kozulin E.M., Pobedonostsev L.A., et al., Yadernye Konstanty, 4/39, 14 (1980).

[67] Smith A.B., Nucl. Phys., 47, 633 (1963).

[68] Maslov V.M., Porodzinskij Yu.V.,Sukhovitskij E.Sh., Proc. Int. Conf. on Neutron Physics, 14-18 Sept., Kiev, USSR, Vol.1, p.413, 1988.

[69] Ignatyuk A.V., Maslov V.M. and Pashchenko A.B., Sov. J. Nucl. Phys., 47, 224 (1988).

[70] Raynal J., Specialists Meeting on the Use of the Optical Model for the calculation of Neutron Cross Sections below 20 MeV, Paris, 13-15 November, NEANDC-222 "U", p.63.

[71] Kanda Y., Kikuchi Y., Nakajima Y. et al., Proc. Int. Conf. Nucl. Data for Sci. and Technology, Julich, Germany, May 13-19, 1991, p.851.

[72] Fröhner F.H., Nucl. Sci. Eng. 103, 119 (1989).

[73] Reference Input Parameter Library, Proc. of IAEA Coordinated Research Program, 1998.

[74] Zhuchko V.E., Ostapenko Yu.B., Smirenkin G.N., Yad. Phys., 28, 1978 (1170).

[75] Stavinskij V.S., Shaker M.O., Nucl. Phys., 62, 667 (1965).

[76] Pöenitz W.P., Proc. of NEANDC/NEACRP Specialist's Meeting on Fast-Neutron Capture Cross Sections, April 20-23, ANL, ANL-83-4, NEANDC(US)-214/L, p.288.

[77] Pöenitz W.P., Fawcett, Jr., L.R. and Smith D.L. Nucl. Sci. Eng. 78, 239 (1981).

[78] Pöenitz W.P., Nucl. Sci. Eng. 57, 300 (1975).

[79] Pöenitz W.P., Nucl. Sci. Eng. (1968).

[80] Kazakov L.E. et al., Yadernye Konstanti, 3, 1986.

[81] Fricke M.P. Lopez W.M., Friesenhahn et al., Proc. Int. Conf. Nuclear Data for Reactors, Helsinki, Finland, June 15-19, 1970, p. 265.

[82] Buleeva N.N., Davletshin A.N., Tipunkov O.A., et al., Atomnaya Energya, 65, 348 (1988).

[83] Lindner M., Nagle R.J. and Landrum J., Nucl. Sci. Eng. 59, 381 (1976).

[84] Quang E., Knoll G.F., Nucl. Sci. Eng. 110, 282 (1991).

[85] Voignier J., Joly S. and Grenier G., Nucl. Sci. Eng. 93, 43 (1986).

[86] Davletshin A.H., Tipunkov A.O. and Tolstikov V.A., Neutron Physics, Proc. All-Union Conference, Vol. 4, p.109, Tsniiatominform, Moscow (1975) [in Russian].

[87] Alkhazov I.D., Kasatkin V.P., Kostochkin O.I., et al., Neutron Physics, Proc. All-Union Conference, Vol. 4, p.13, Tsniiatominform, Moscow (1973) [in Russian].

[88] Lisowski P.W., Gavron A., Parker W.E. et al. Proc. Specialists' Meeting on Neutron Cross Section Standards for the Energy Region above 20 MeV, Uppsala, Sweden, May 21-23, 1991, p. 177, OECD, Paris, 1991.

[89] Boykov G.S., Dmitriev V.D., Kudyaev G.A., Maslov V.M., et al., Ann. Nucl. Energy, 10, 585 (1994).

[90] McNally J.H., Barnes J.W., Dropesky B.J. et al., Phys. Rev. C9, 717 (1974).

[91] Kornilov N.V., Yadernie Konstanti, 4, 46 (1985).

[92] Baba M., J. Nucl. Sci. Tech., 27, 601 (1989).

[93] Porodzinskij Yu.V., Sukhovitskij E.Sh., Selected Papers of ISTC Workshop on Nuclear Data of Minor Actinides, May 27-31, JAERI, Tokai, Japan, JAERI-Conf, 97-001, p. 25.

[94] Porodzinskij Yu.V., Sukhovitskij E.Sh., Proc. Int. Conf. Nucl. Data for Sci. and Technology, Trieste, Italy, May 19-23, 1997.

[95] Kornilov N.V., Zhuravlev B.V., Salnikov O.A., et al., Atomnaya Energya, 49, 283 (1980).

[96] Frehaut J, Mosinski G., Proc. Conf. Nuclear Cross Sections and Technology, Washington D.C., March 3-7, 1975, CONF-750303, Vol. 2, p.855, US National Bureau of Standards (1975).

[97] Frehaut J., Bertin A., Bois R., Nucl. Sci. Eng. 74, 29 (1980).

[98] Kornilov N.V., Vinogradov V.N., Gai E.V. et al., Yadernie Konstanti, 41,1(45) (1982).

[99] Kornilov N.V., Vinogradov V.N., Gai E.V. et al., Proc. Int. Conf. Nucl. Data for Sci. and Technology, Antwerpen, September 6-10, 1982, p.679.

[100] Karius H., Ackermann A., Scobel W., Journ. Phys., G, 5, 715 (1979).

[101] Veeser L.R., Arthur E.D., Neutron Physics and Nuclear Data, OECD, Harwell, 1054 (1978).

[102] Chou You-Pu, HSJ-77091 (1976).

[103] Landrum J.H., Nagel R.J., Lindner M., Phys. Rev. C, 8, 1938 (1973).

[104] Golovnya V.Ya., Goncharov K.S., Dolya G.P., et al., Proc. Int. Conf. on Neutron Physics, September14-18, 1987, Kiev, USSR, Vol.3, p.281, 1988.

[105] Maslov V.M. and Hasegawa A., Third Specialists Meeting on High Energy Nuclear Data, March 30-31, 1998, JAERI, Tokai, Japan.

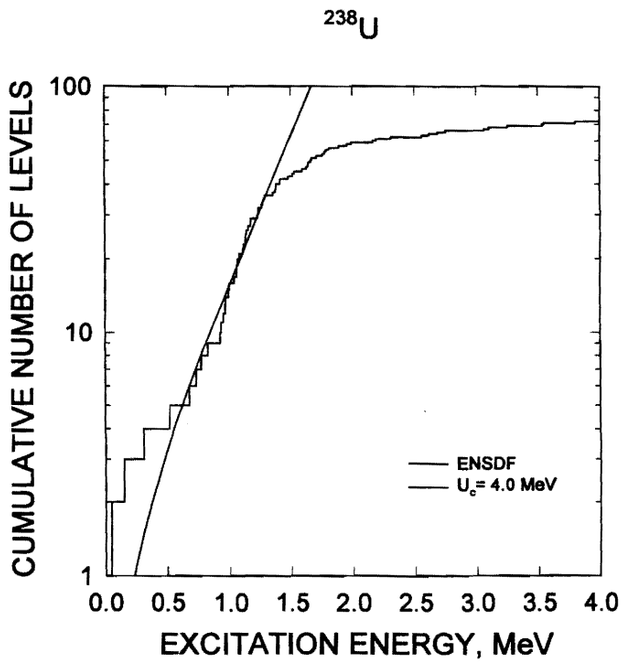

Fig. 1 Cumulative number of levels of ^{238}U.

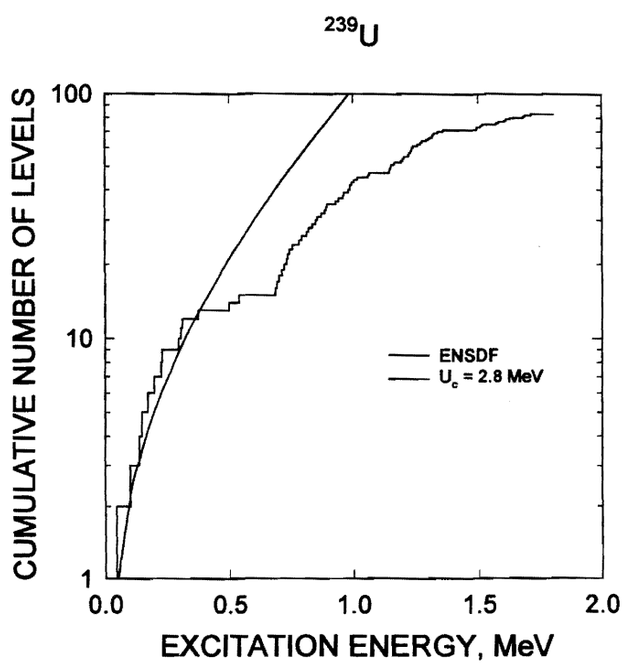

Fig. 2 Cumulative number of levels of ^{239}U.

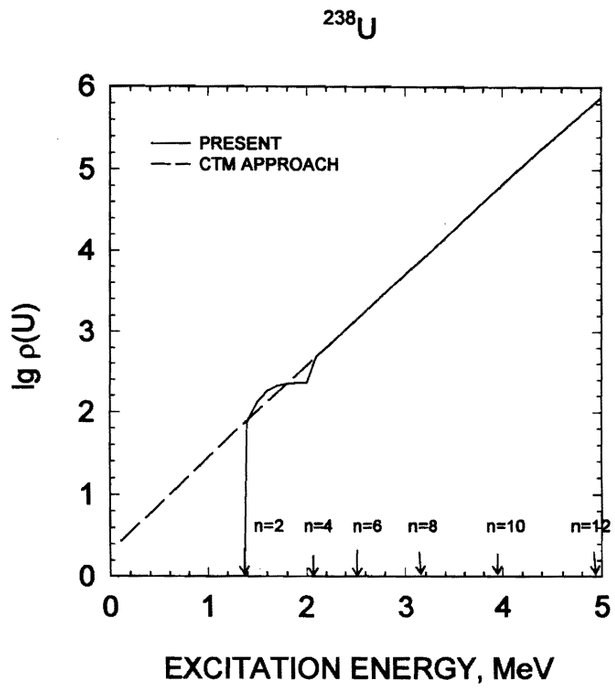

Fig. 3 Level density of ^{238}U.

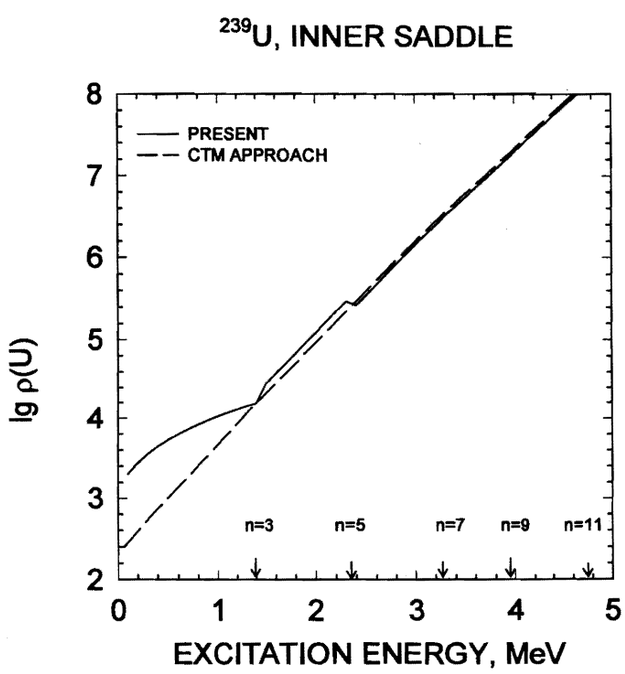

Fig. 4 Level density of ^{239}U.

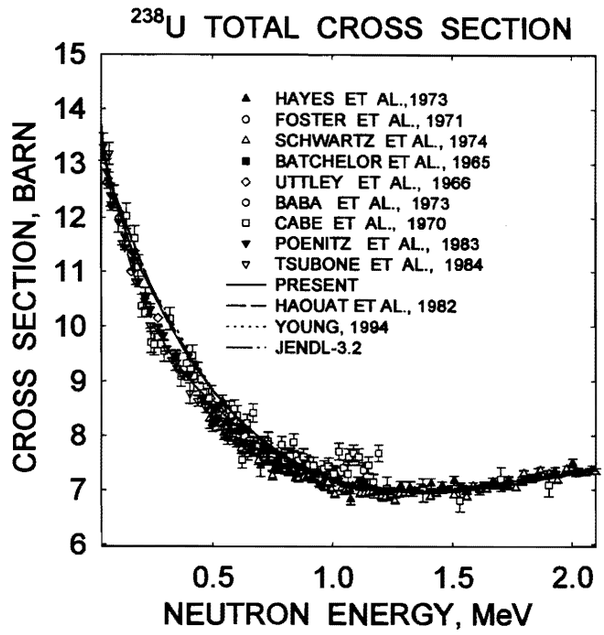

Fig. 5 Total cross section of ^{238}U.

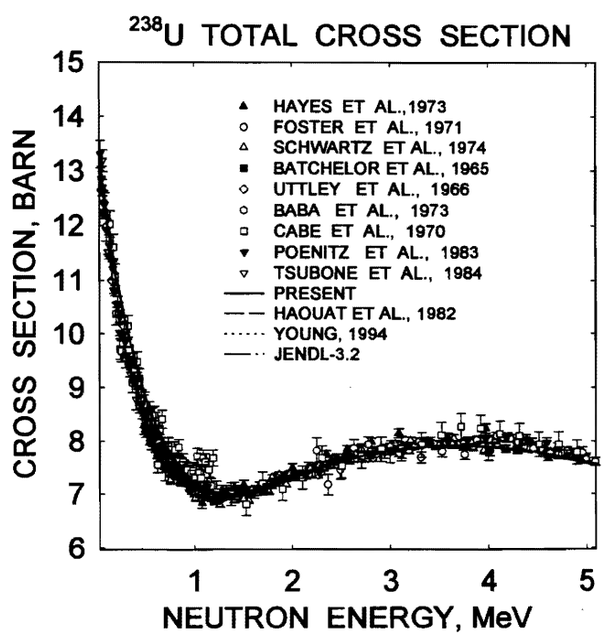

Fig. 6 Total cross section of ^{238}U.

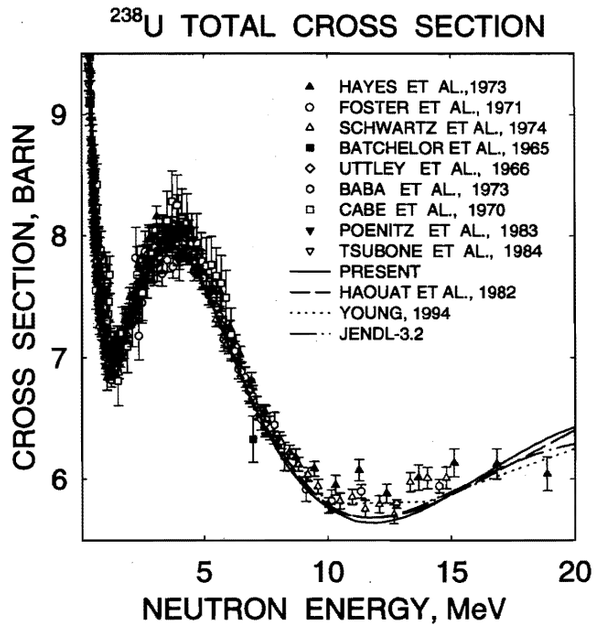

Fig. 7 Total cross section of ^{238}U.

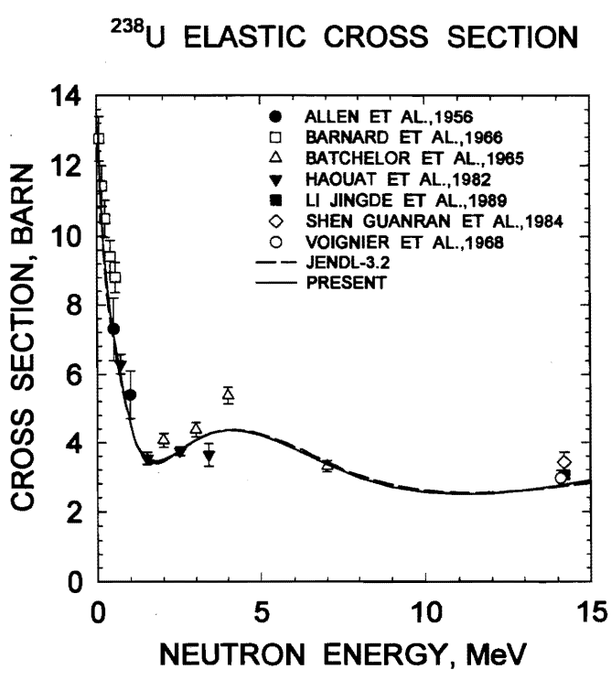

Fig. 8 Elastic scattering cross section of ^{238}U.

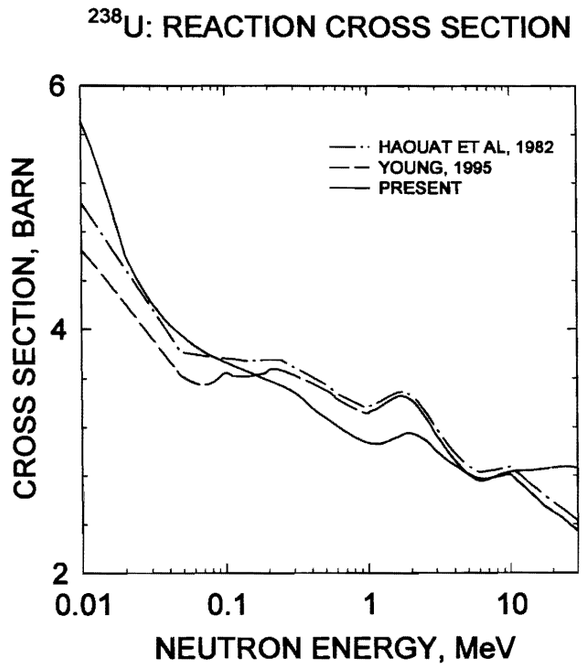

Fig. 9 Reaction cross section of ^{238}U.

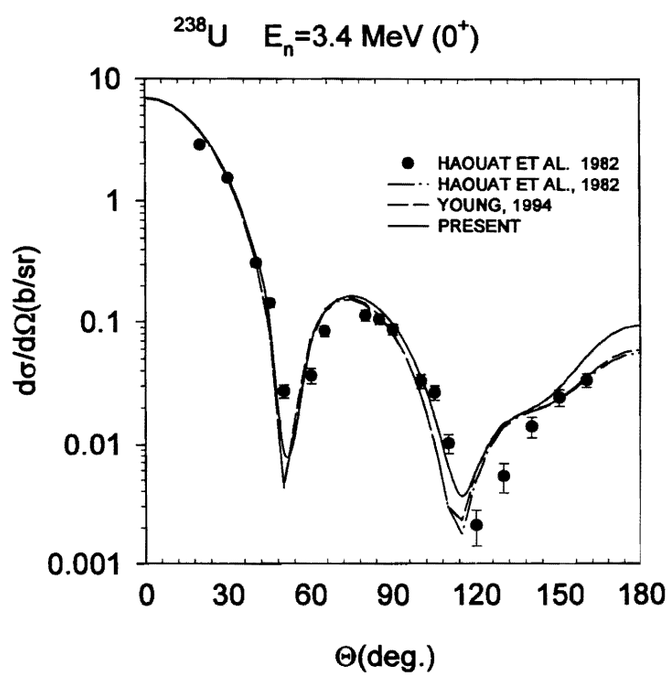

Fig. 10 Differential elastic scattering cross section at 3.4 MeV.

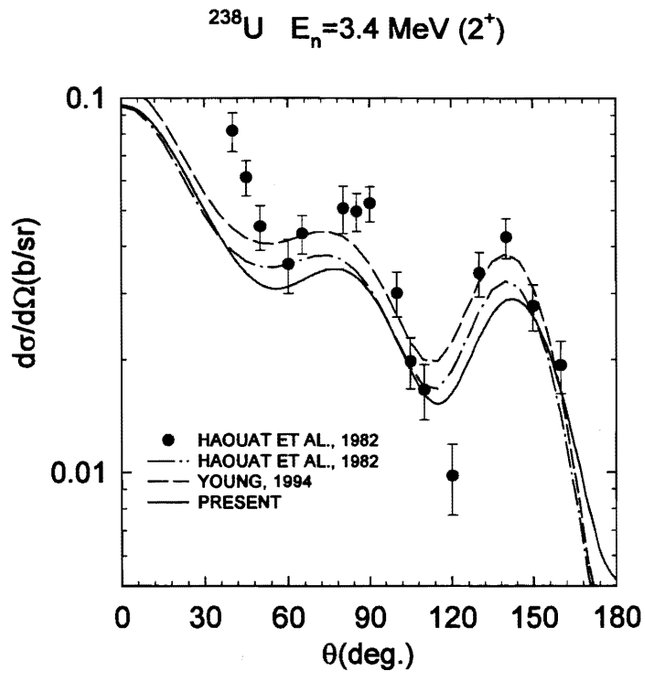

Fig. 11 Differential inelastic scattering cross section to 2^+ level at 3.4 MeV.

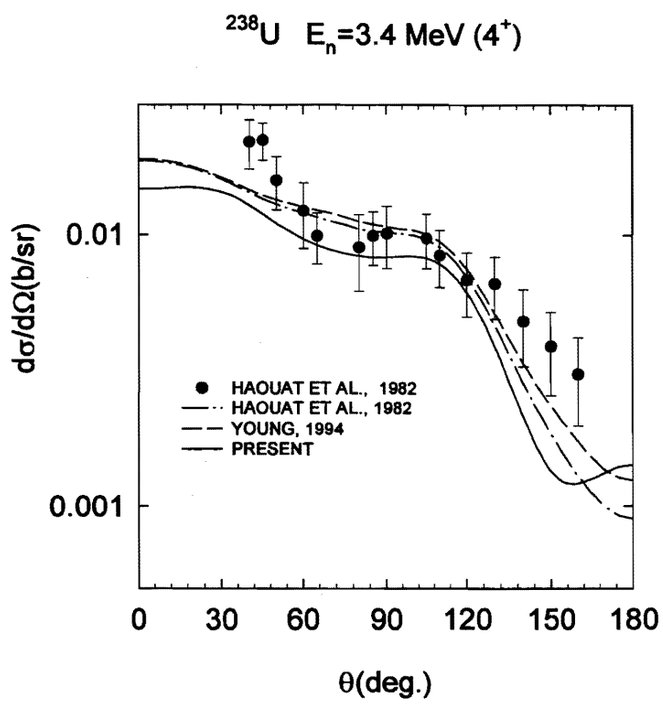

Fig. 12 Differential inelastic scattering cross section to 4^+ level at 3.4 MeV.

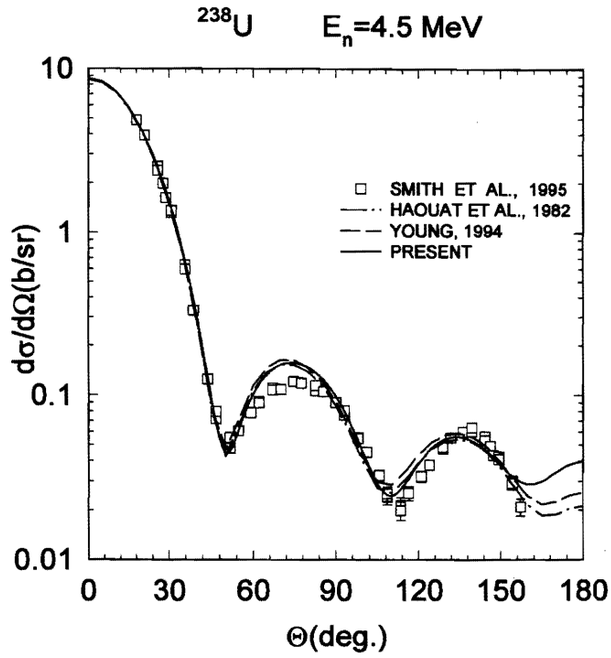

Fig. 13 Differential elastic scattering cross section at 4.5 MeV.

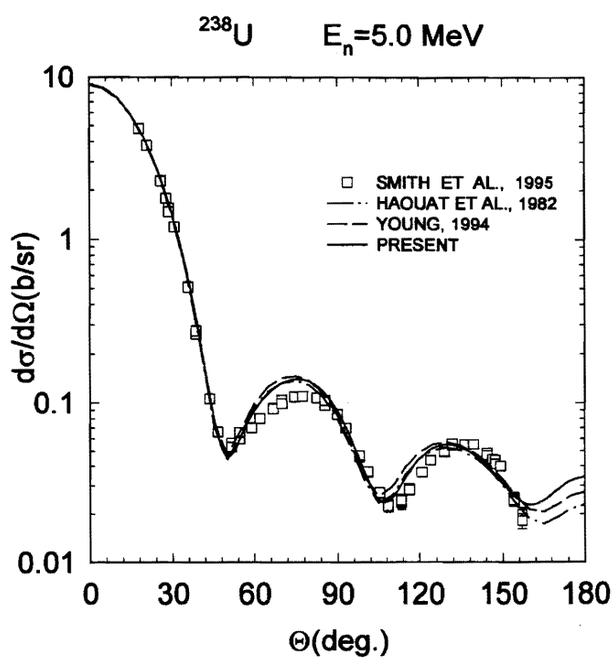

Fig. 14 Differential elastic scattering cross section at 5.0 MeV.

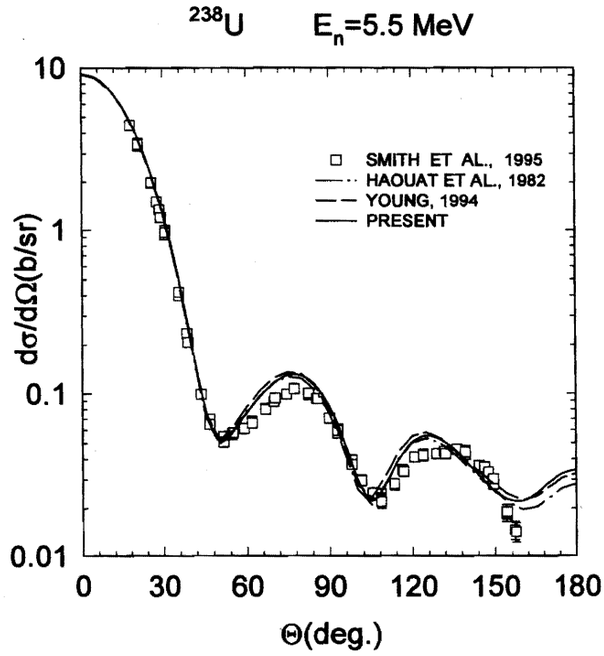

Fig. 15 Differential elastic scattering cross section at 5.5 MeV.

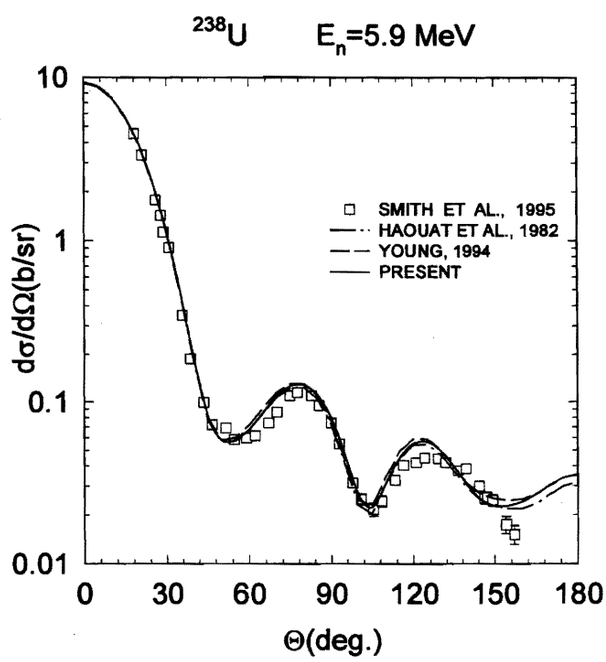

Fig. 16 Differential elastic scattering cross section at 5.9 MeV.

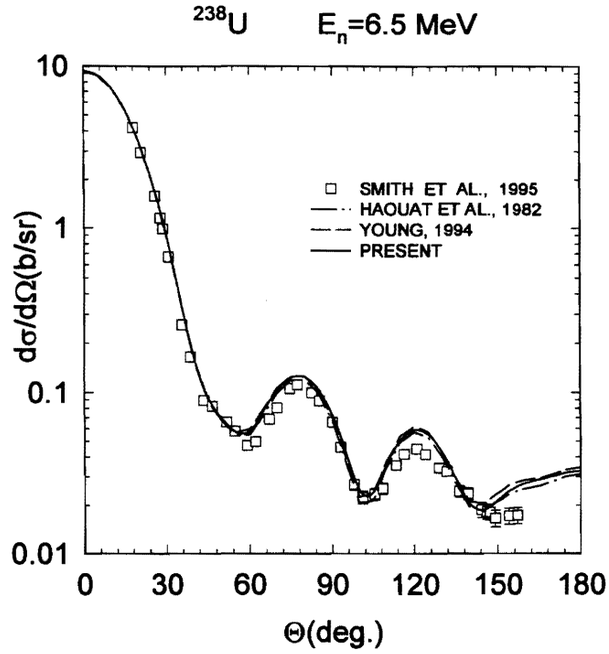

Fig. 17 Differential elastic scattering cross section at 6.5 MeV.

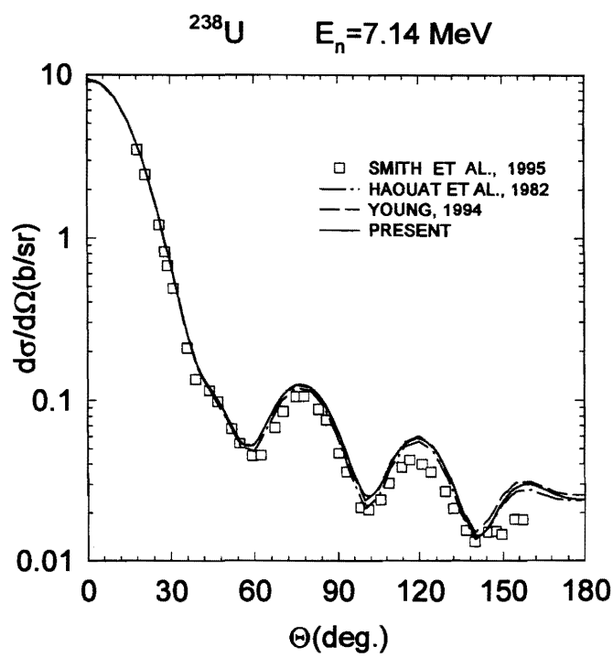

Fig. 18 Differential elastic scattering cross section at 7.14 MeV.

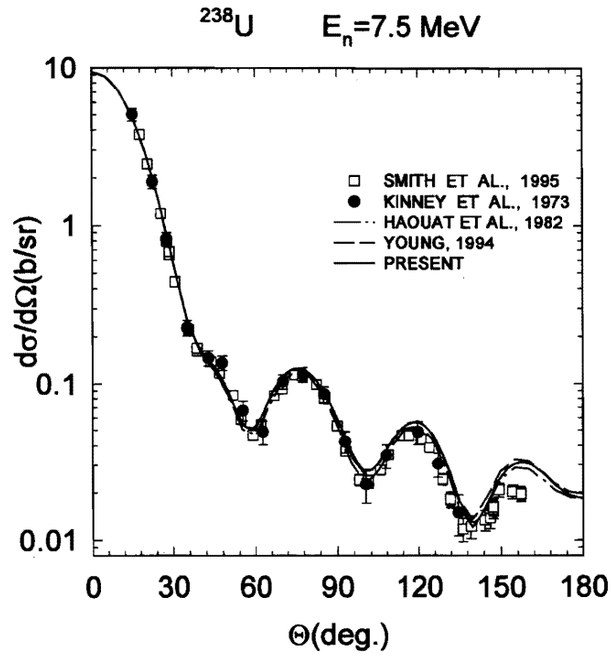

Fig. 19 Differential elastic scattering cross section at 7.5 MeV.

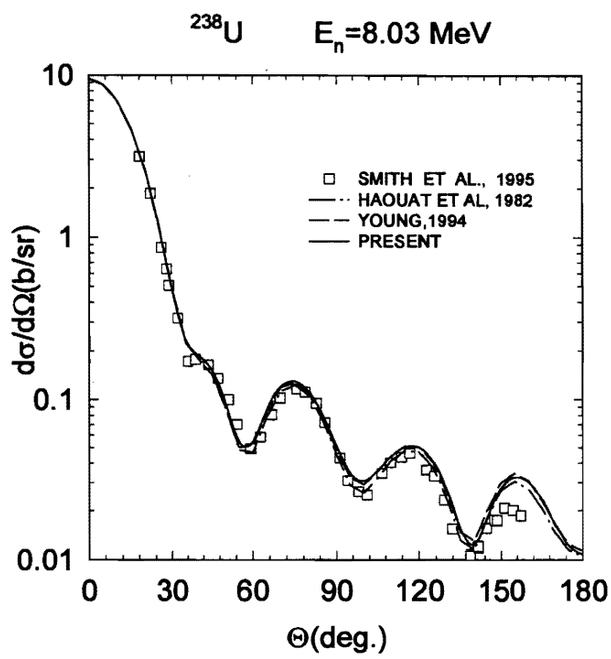

Fig. 20 Differential elastic scattering cross section at 8.03 MeV.

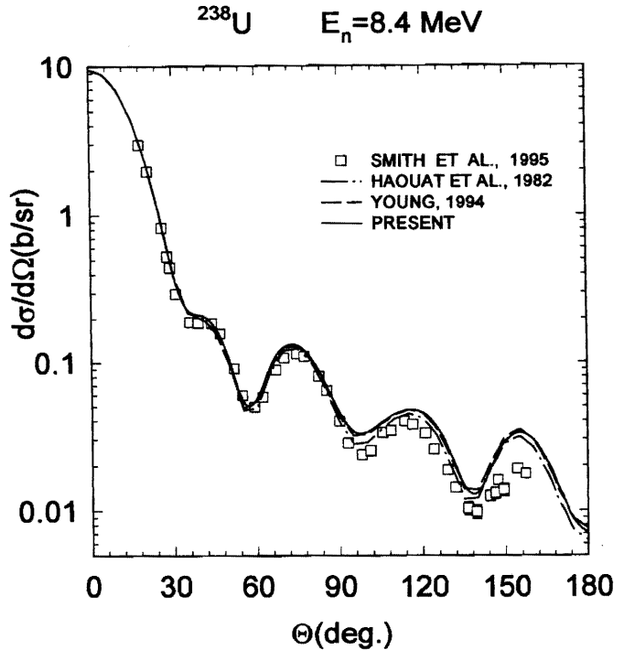

Fig. 21 Differential elastic scattering cross section at 8.4 MeV.

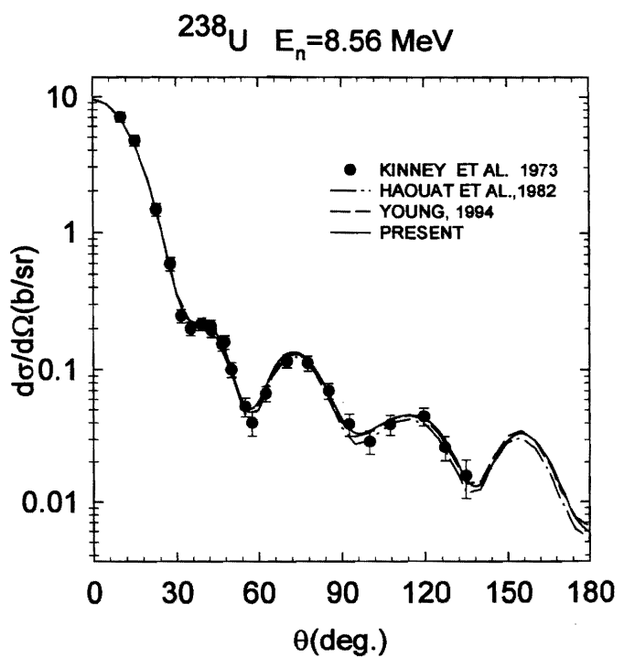

Fig. 22 Differential elastic scattering cross section at 8.56 MeV.

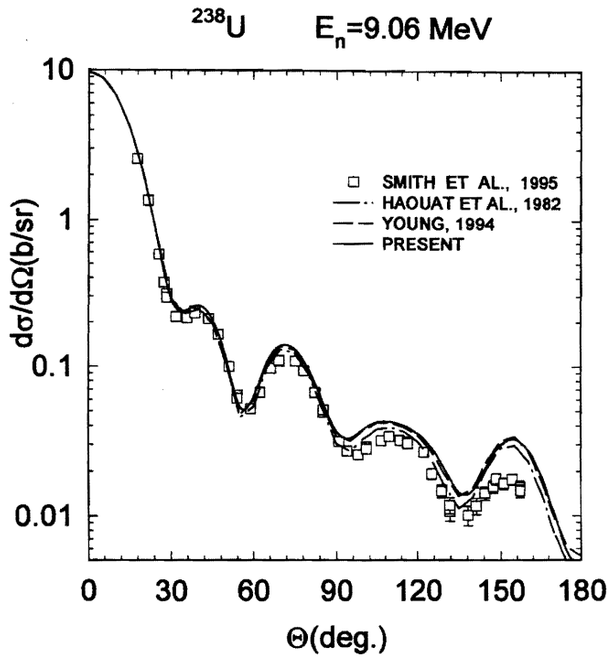

Fig. 23 Differential elastic scattering cross section at 9.06 MeV.

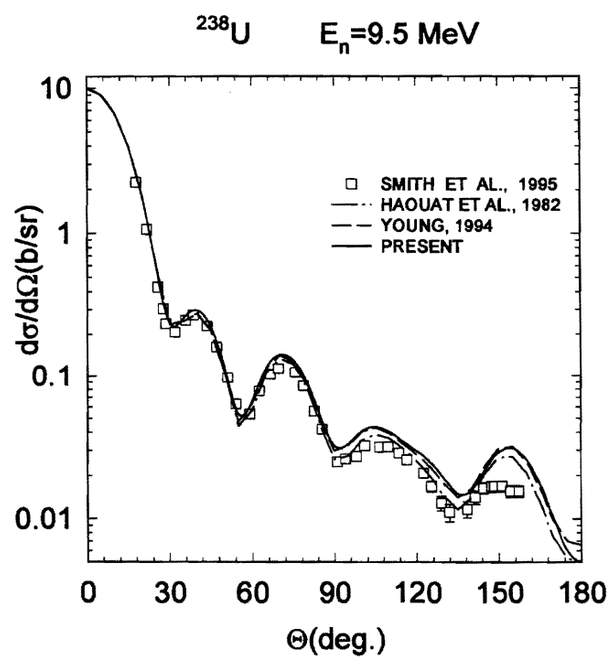

Fig. 24 Differential elastic scattering cross section at 9.5 MeV.

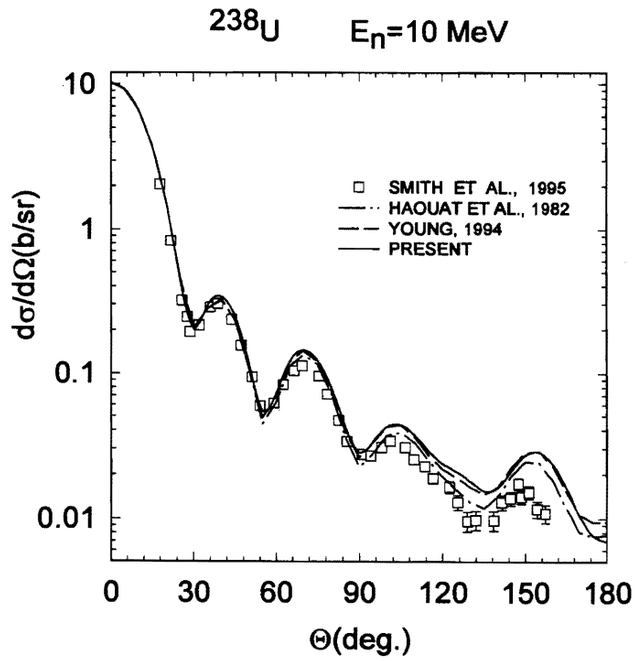

Fig. 25 Differential elastic scattering cross section at 10 MeV.

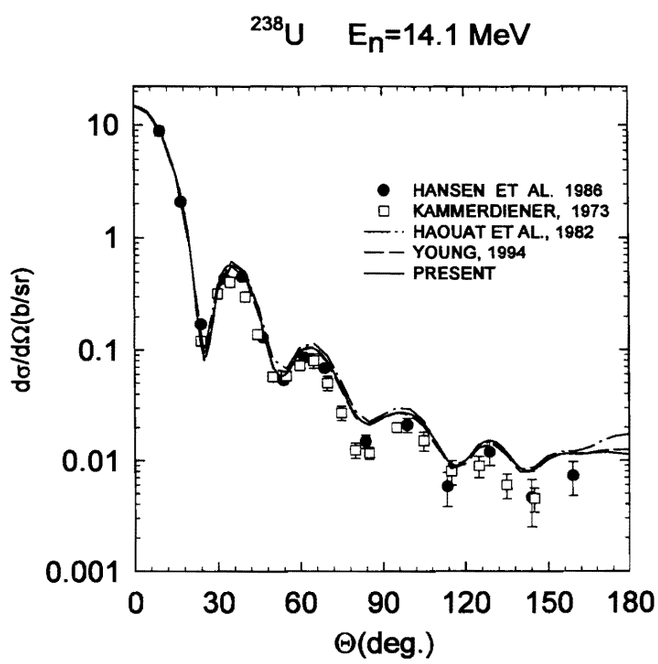

Fig. 26 Differential elastic scattering cross section at 14.1 MeV.

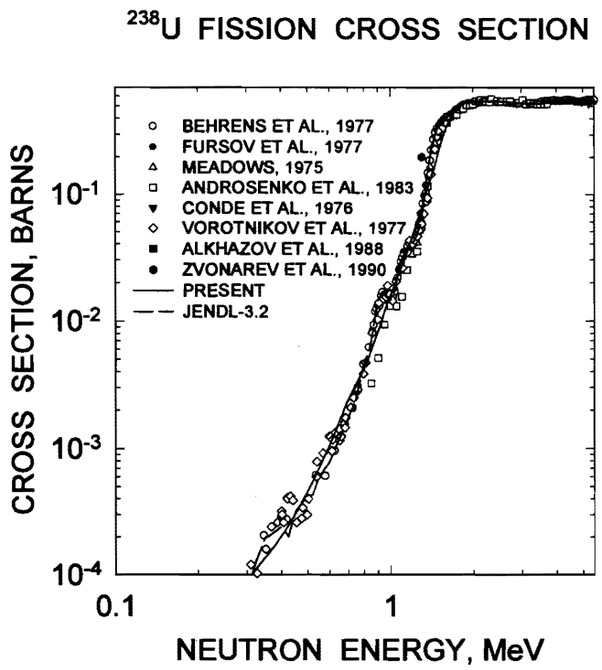

Fig. 27 Fission cross section of ^{238}U.

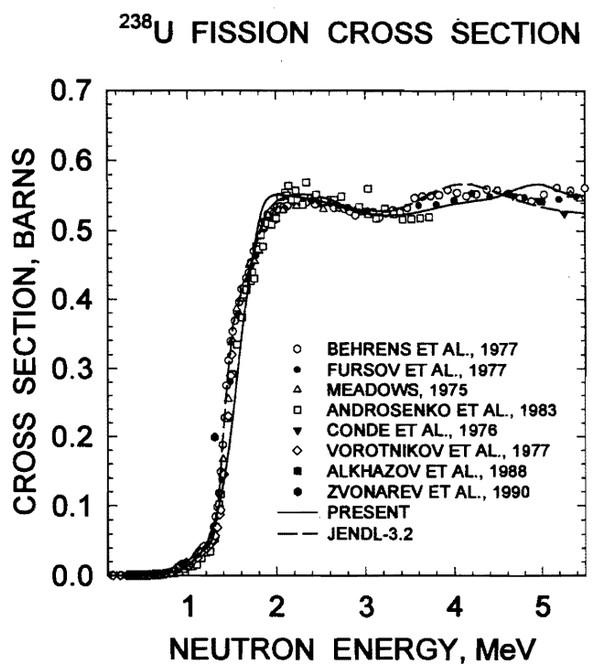

Fig. 28 Fission cross section of ^{238}U.

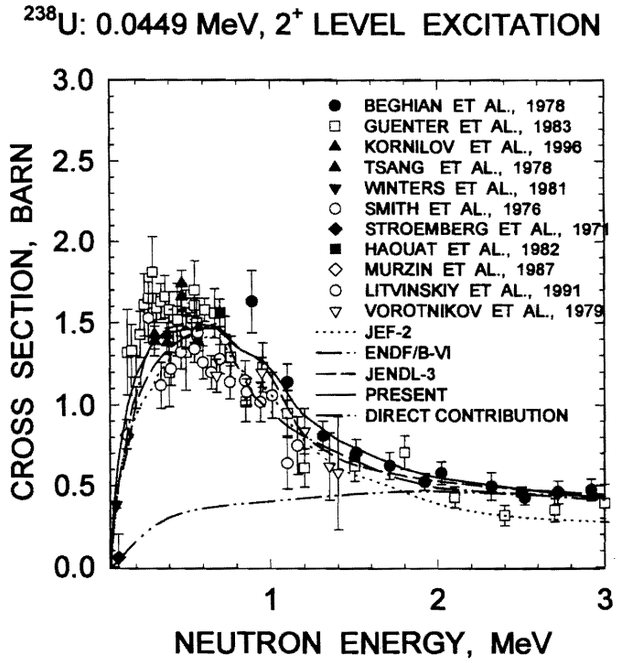

Fig. 29 Cross section of ^{238}U: 0.0449 MeV, 2^+ level excitation.

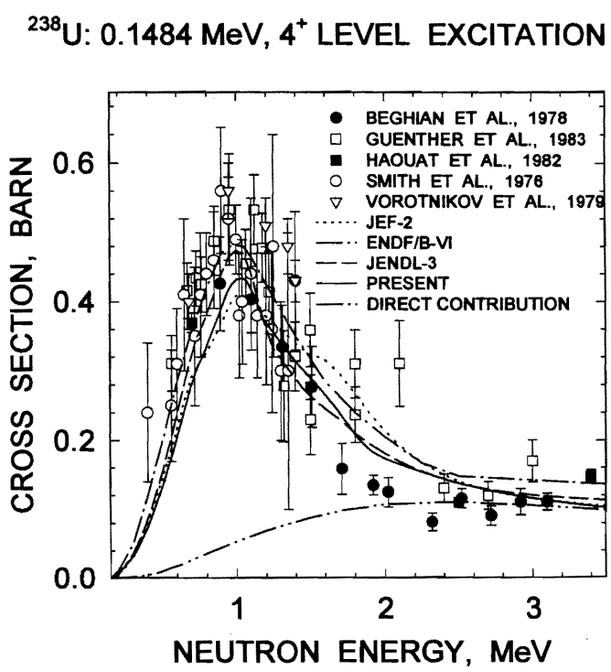

Fig. 30 Cross section of ^{238}U: 0.1484 MeV, 4^+ level excitation.

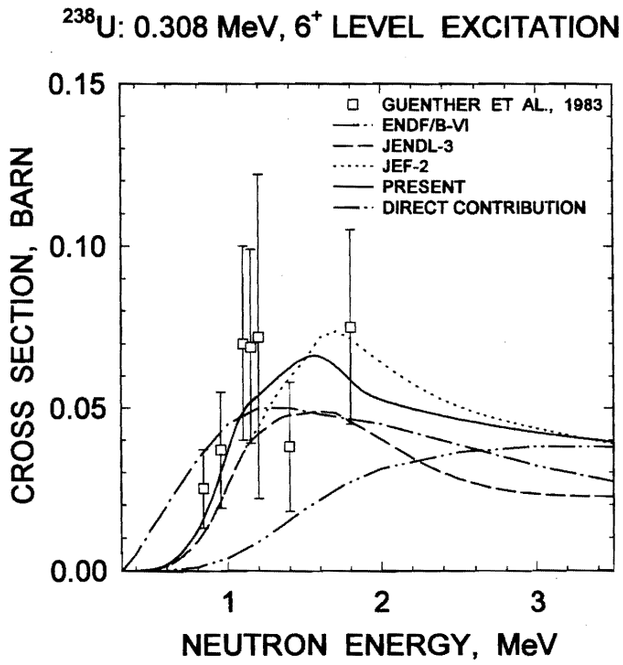

Fig. 31 Cross section of ^{238}U: 0.308 MeV, 6^+ level excitation.

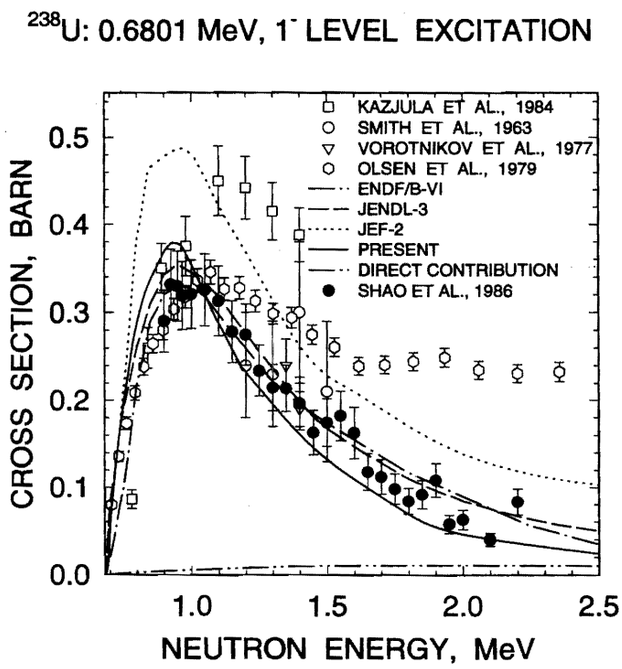

Fig. 32 Cross section of ^{238}U: 0.6801 MeV, 1^- level excitation.

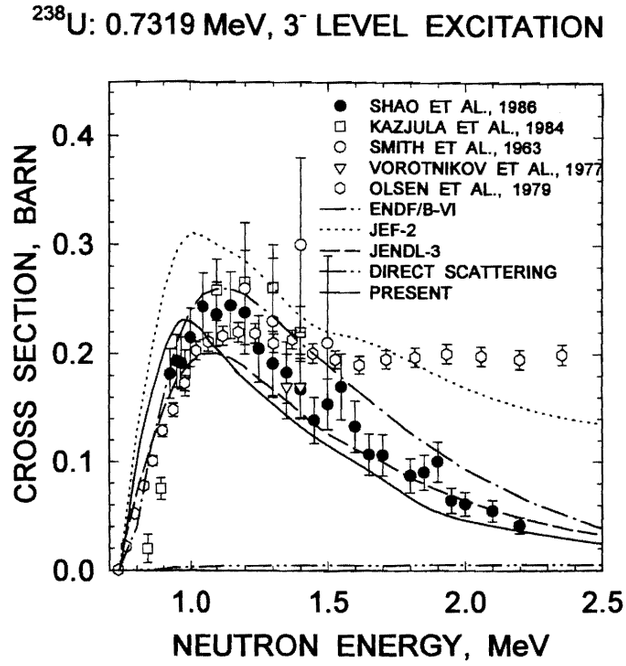

Fig. 33 Cross section of ^{238}U: 0.7319 MeV, 3^- level excitation.

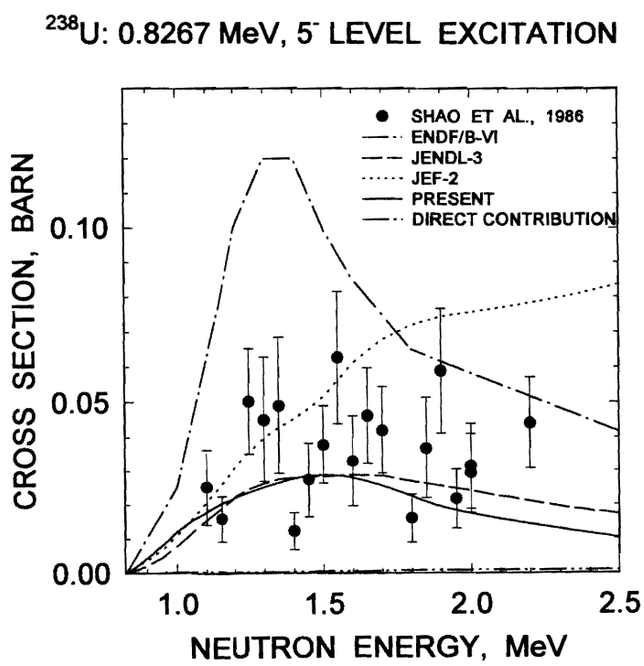

Fig. 34 Cross section of ^{238}U: 0.8267 MeV, 5^- level excitation.

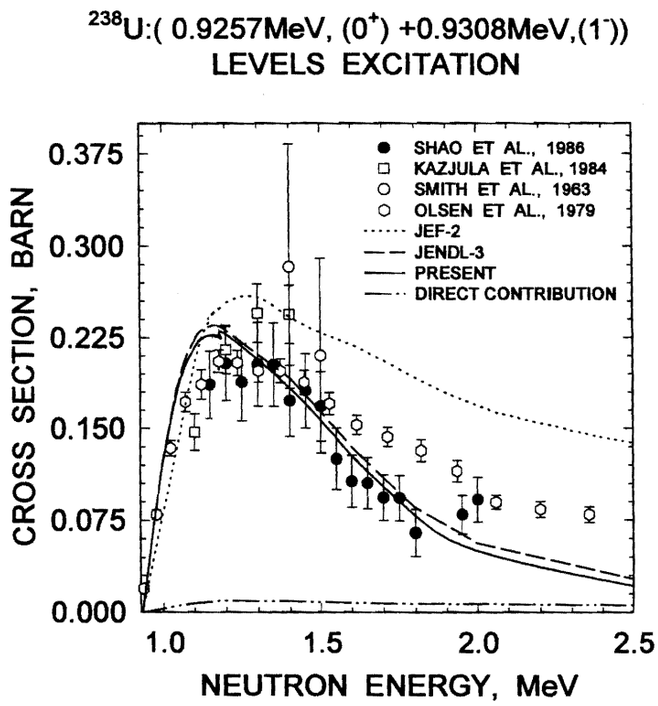

Fig. 35 Cross section of ^{238}U: 0.9257 MeV, 0^+ and 0.9308 MeV, 1^- levels excitation.

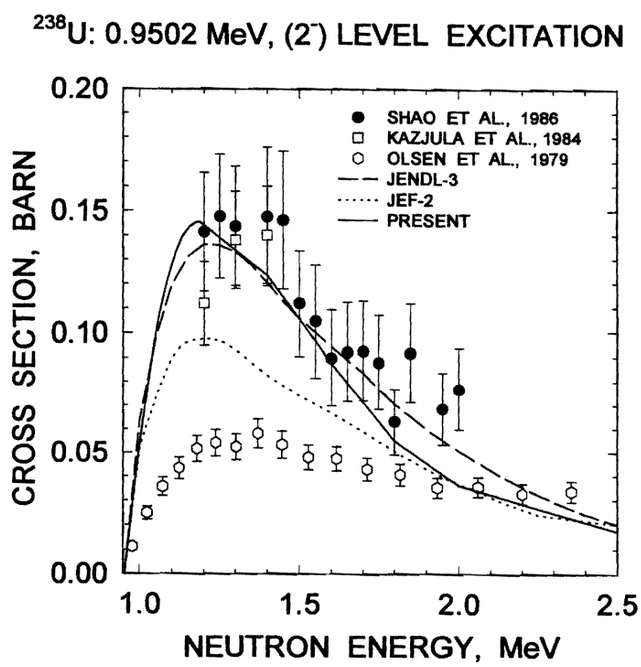

Fig. 36 Cross section of ^{238}U: 0.9502 MeV, 2^- level excitation.

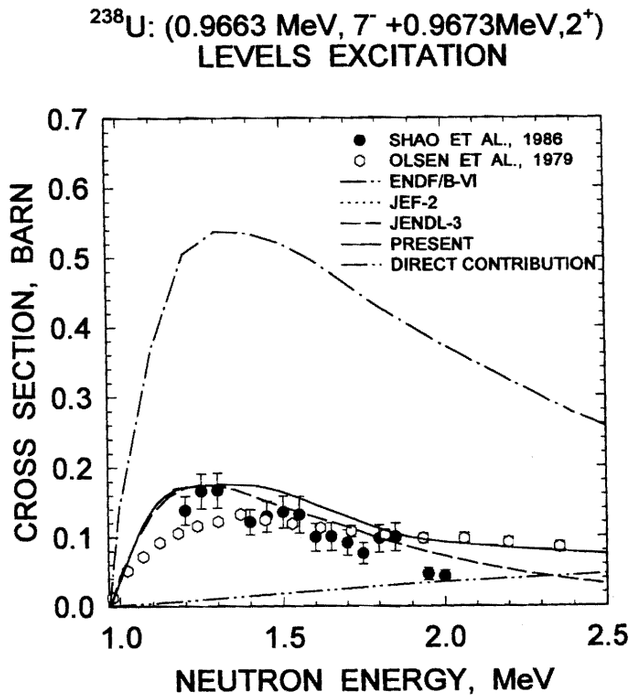

Fig. 37 Cross section of ^{238}U: 0.9663 MeV, 7^- and 0.9673 MeV, 2^+ levels excitation.

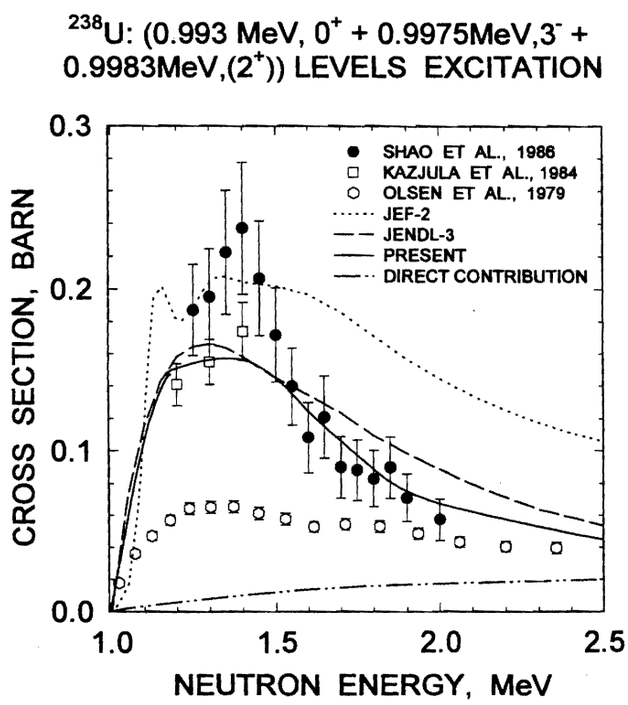

Fig. 38 Cross section of ^{238}U: 0.993 MeV, 0^+,0.9975 MeV, 3^- and 0.9983 MeV 2^+ levels excitation.

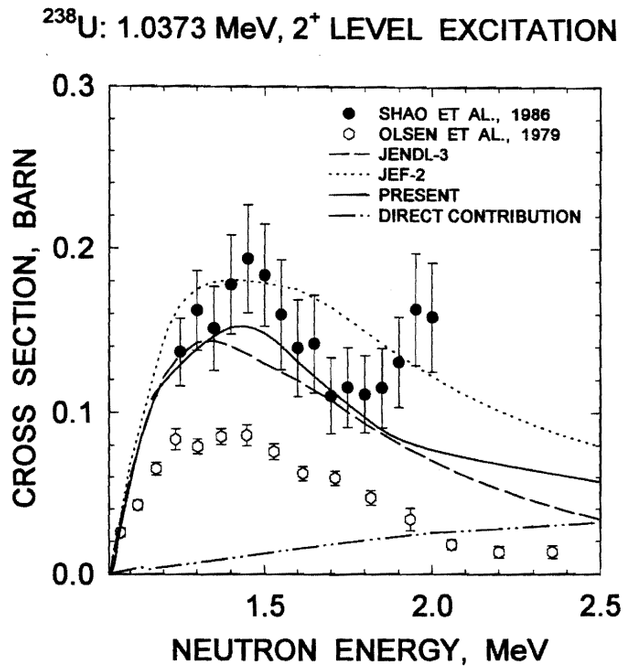

Fig. 39 Cross section of ^{238}U: 1.0373 MeV, 2^+ level excitation.

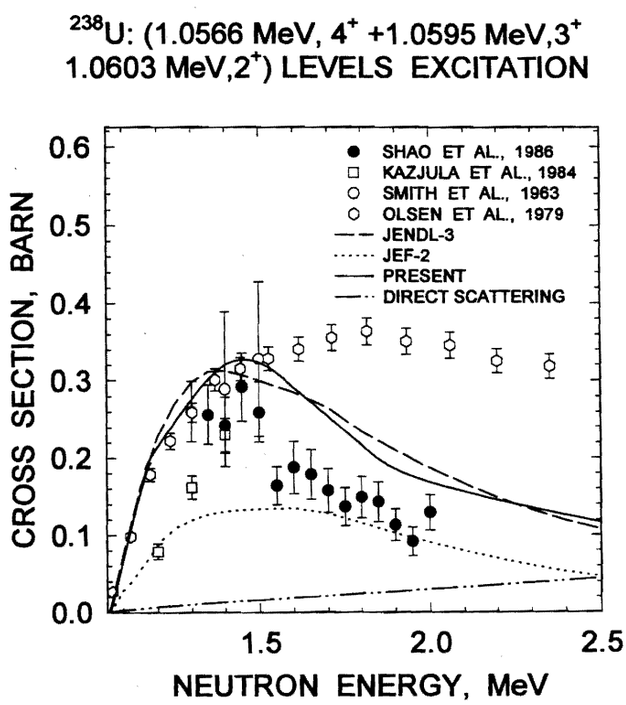

Fig. 40 Cross section of ^{238}U: 1.0566 MeV, 4^+, 1.0595 MeV, 3^+ and 1.0603, 2^+ levels excitation.

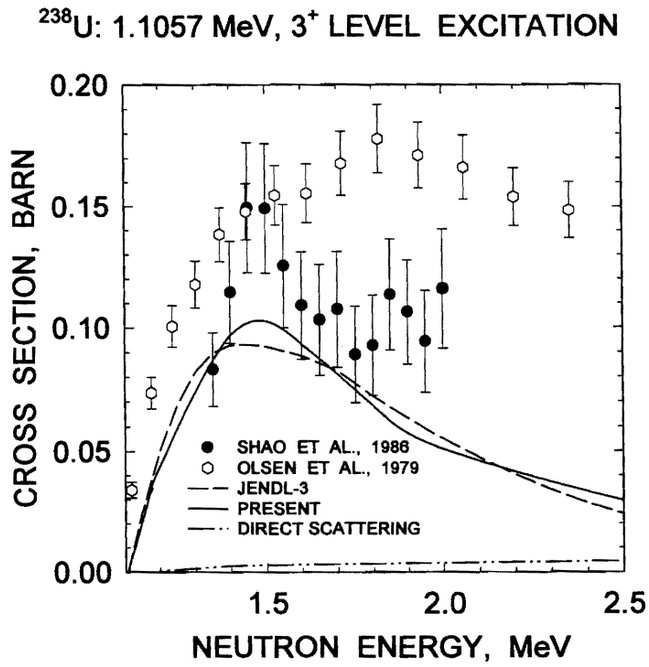

Fig. 41 Cross section of ^{238}U: 1.1057 MeV, 3^+ level excitation.

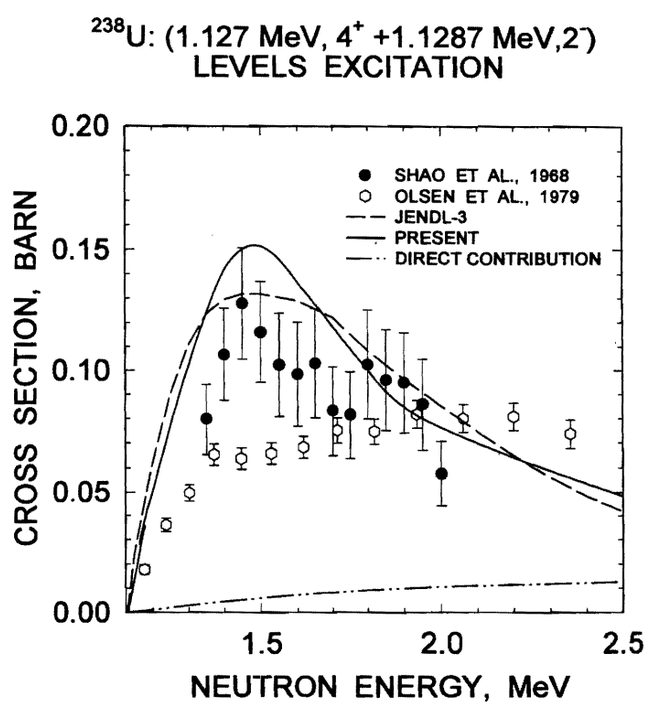

Fig. 42 Cross section of ^{238}U: 1.127 MeV, $4^+$and 1.1287 MeV, 2^- levels excitation.

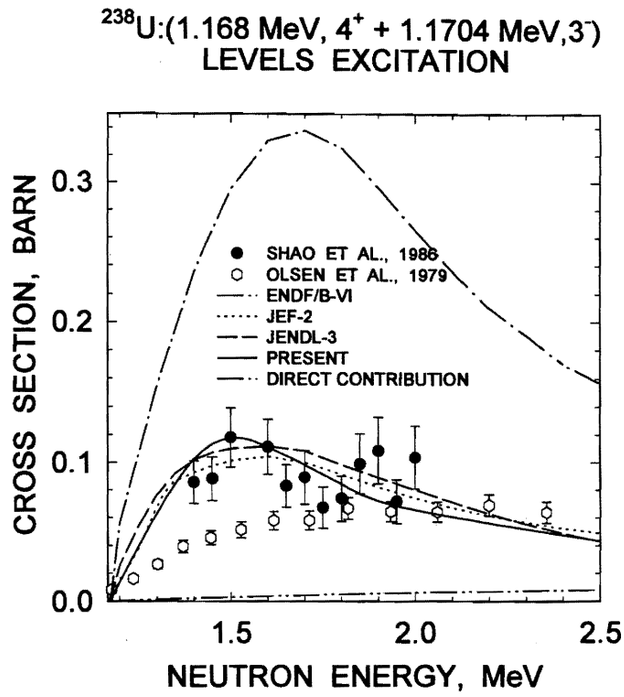

Fig. 43 Cross section of ^{238}U: 1.168 MeV, $4^+$and 1.1704 MeV, 3^- levels excitation.

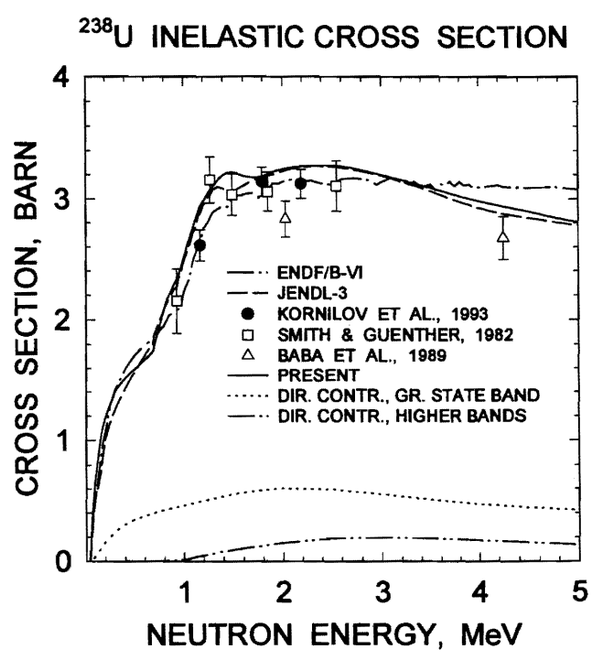

Fig. 44 Inelastic scattering cross section of ^{238}U.

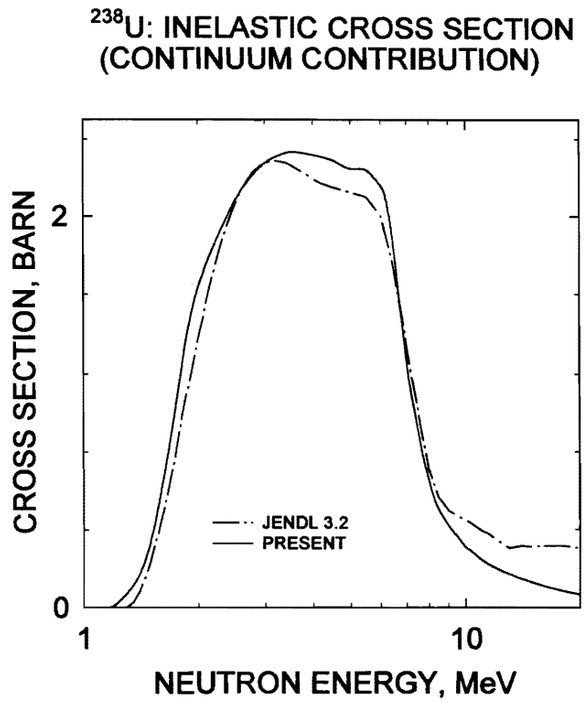

Fig. 45 Inelastic scattering cross section of ^{238}U.

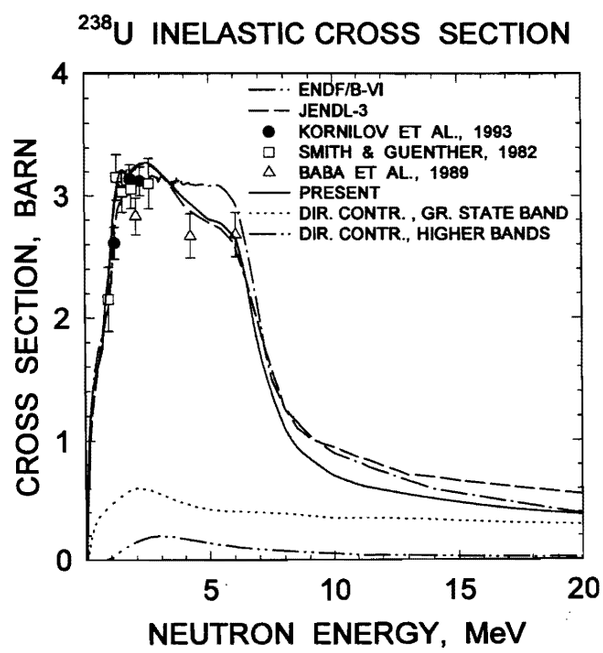

Fig. 46 Inelastic scattering cross section of ^{238}U.

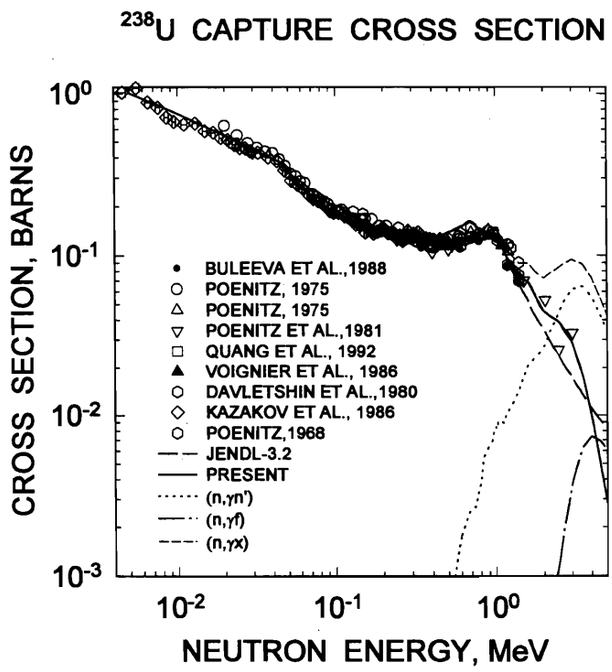

Fig. 47 Capture cross section of ^{238}U.

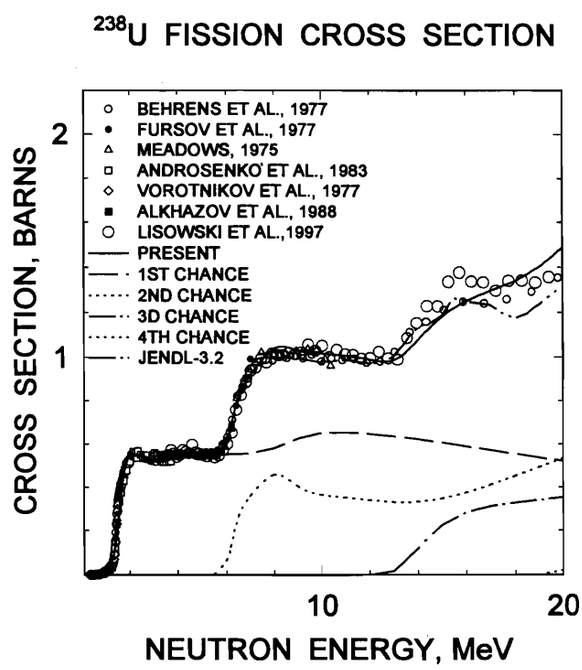

Fig. 48 Fission cross section of ^{238}U.

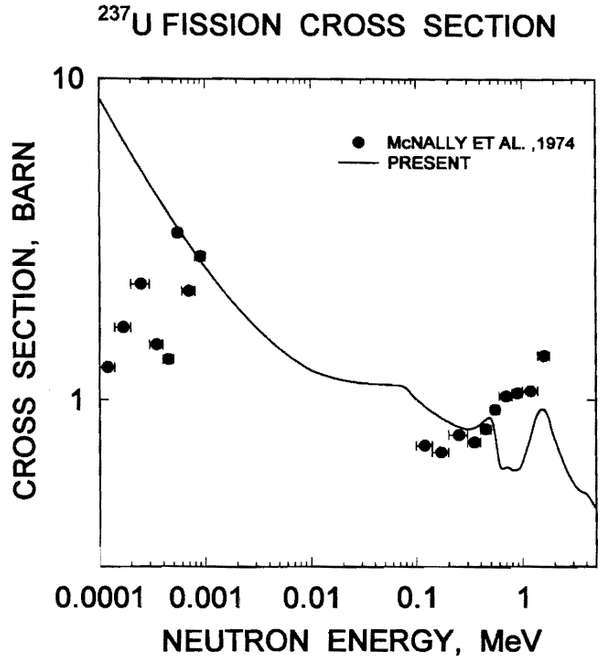

Fig. 49 Fission cross section of ^{237}U.

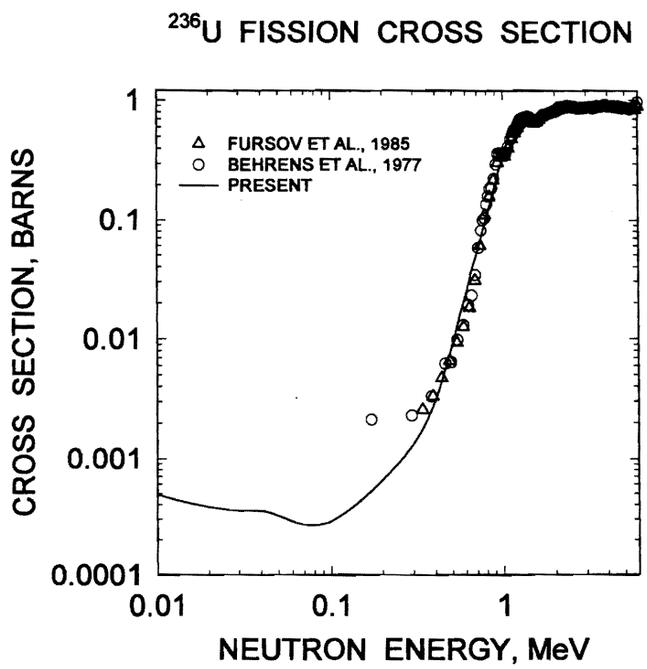

Fig. 50 Fission cross section of ^{236}U.

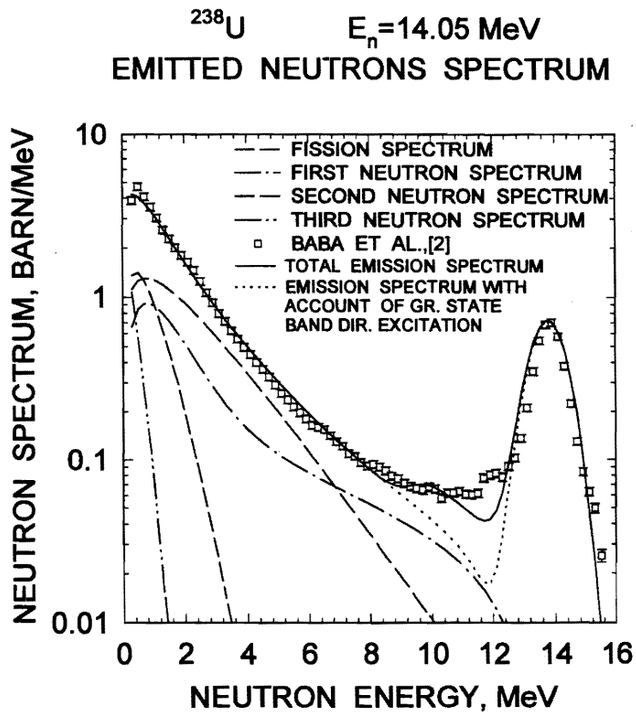

Fig. 51 Neutron spectrum of ^{238}U for incident neutron energy 14 MeV.

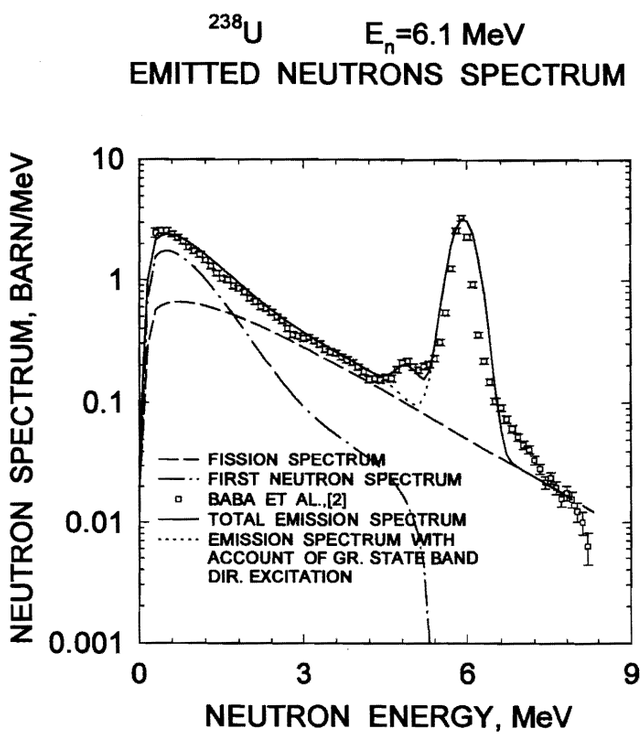

Fig. 52 Neutron spectrum of ^{238}U for incident neutron energy 6.1 MeV.

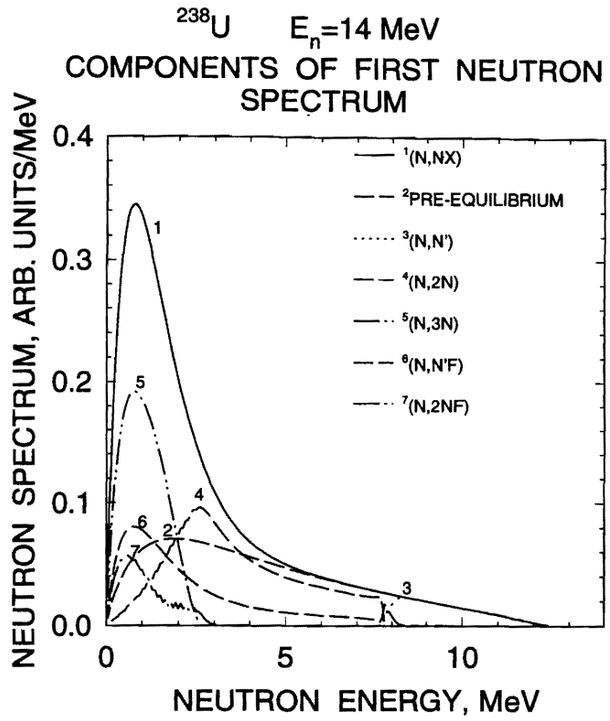

Fig. 53 Components of first neutron spectrum of ^{238}U for incident neutron energy 14 MeV.

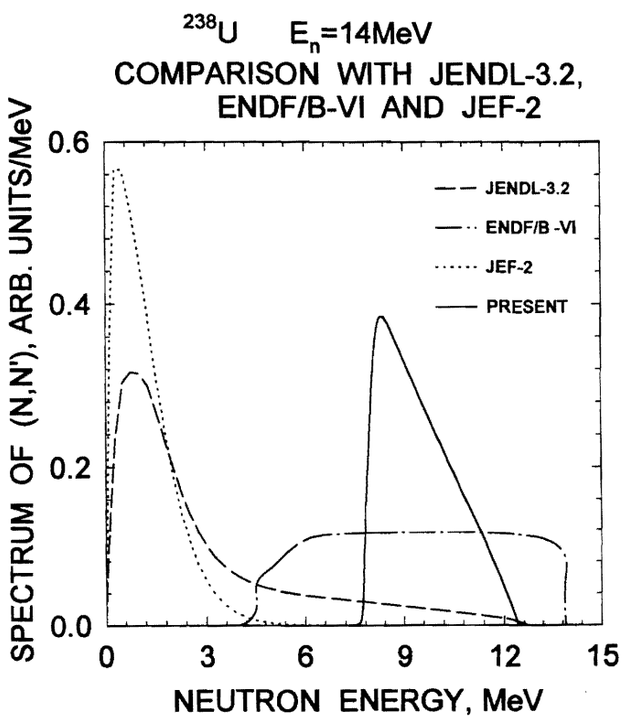

Fig. 54 Comparison of (n,n'γ) reaction neutron spectra of ^{238}U for incident neutron energy 14 MeV.

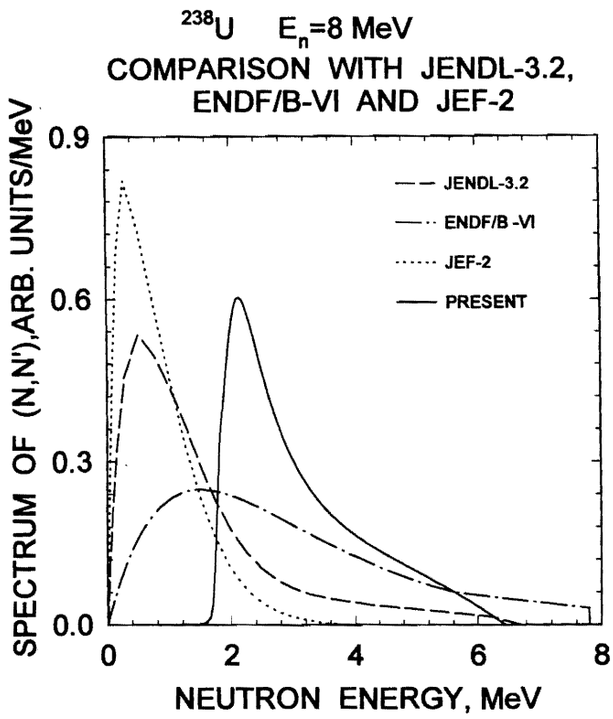

Fig. 55 Comparison of (n,n'γ) reaction neutron spectra of ^{238}U for incident neutron energy 8 MeV.

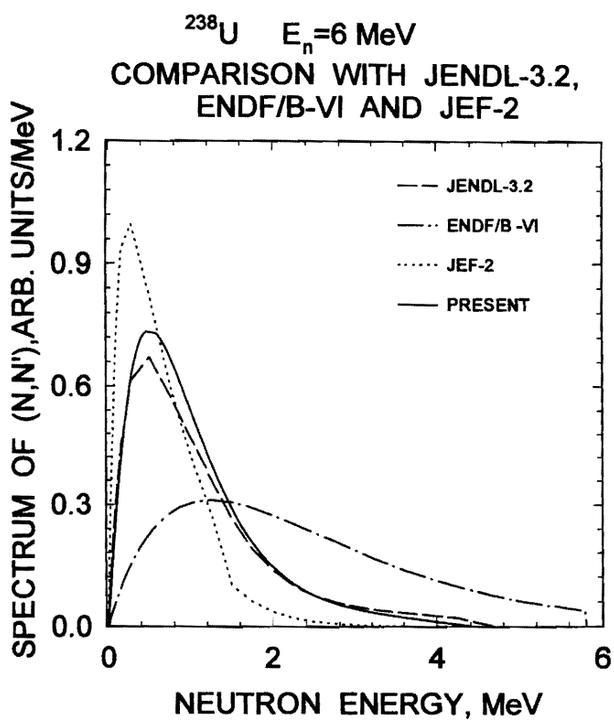

Fig. 56 Comparison of (n,n'γ) reaction neutron spectra of ^{238}U for incident neutron energy 6 MeV.

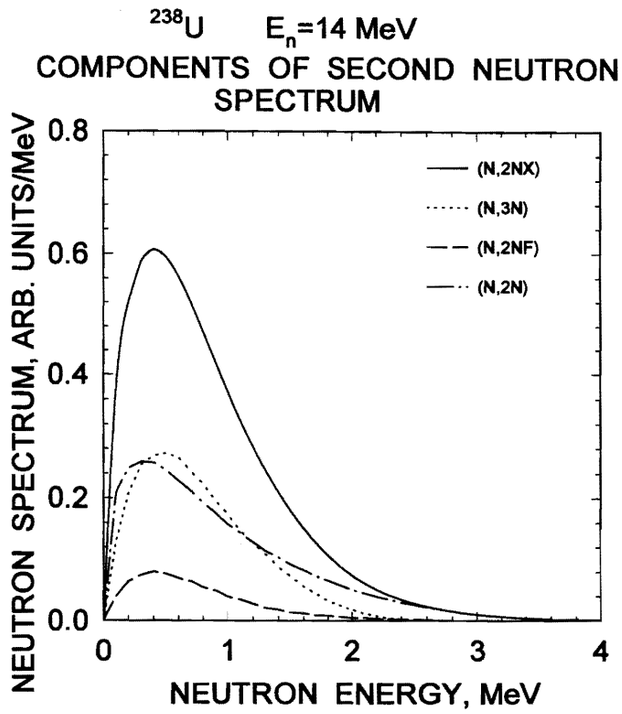

Fig. 57 Components of second neutron spectrum of ^{238}U for incident neutron energy 14 MeV.

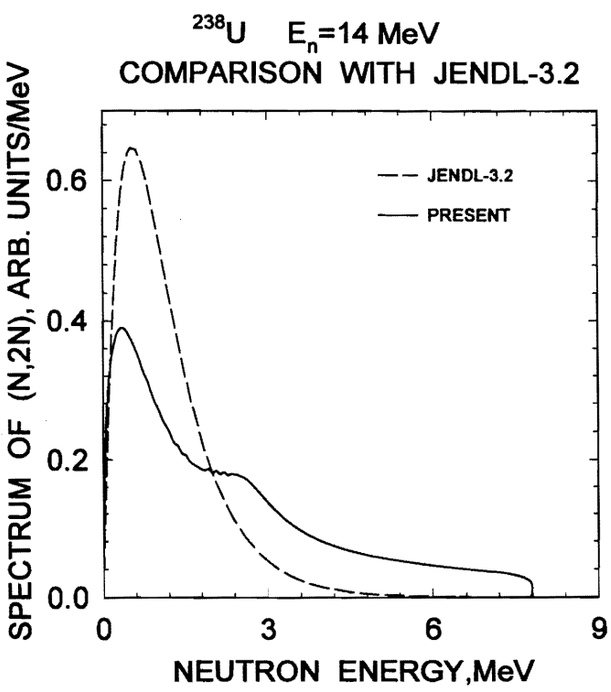

Fig. 58 Comparison of (n,2n) reaction neutron spectra of ^{238}U for incident neutron energy 14 MeV.

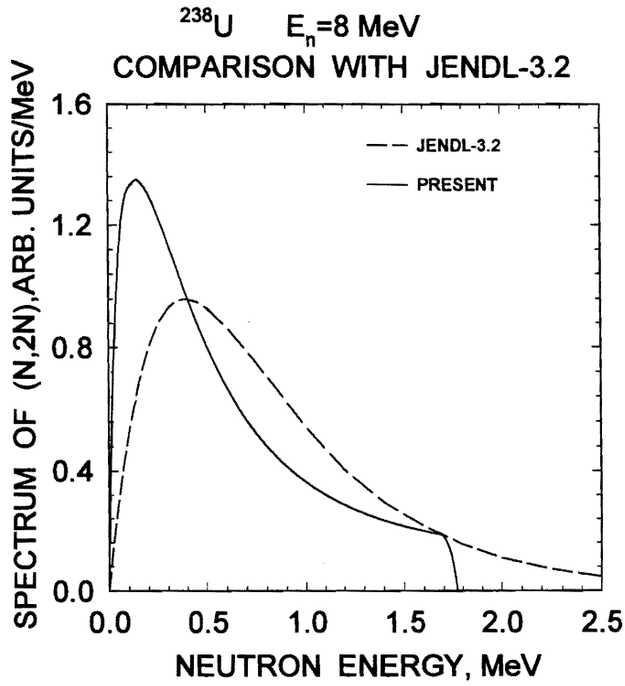

Fig. 59 Comparison of (n,2n) reaction neutron spectra of ^{238}U for incident neutron energy 8 MeV.

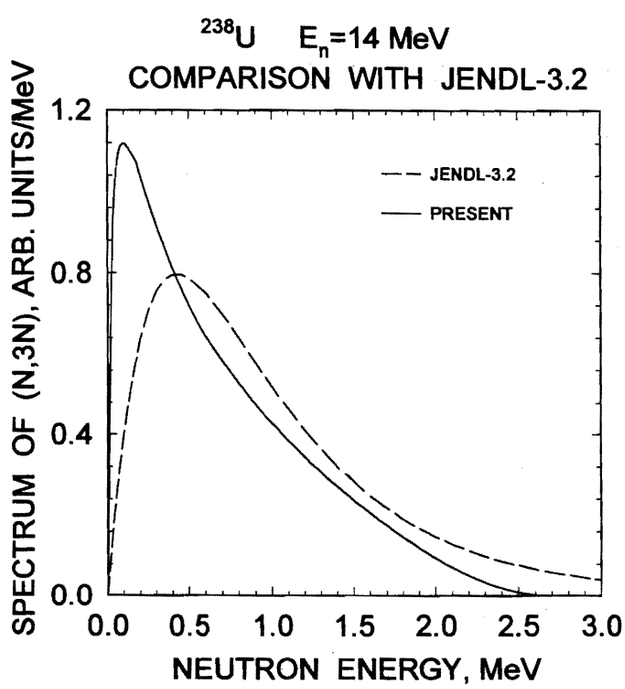

Fig. 60 Comparison of (n,3n) reaction neutron spectra of ^{238}U for incident neutron energy 14 MeV..

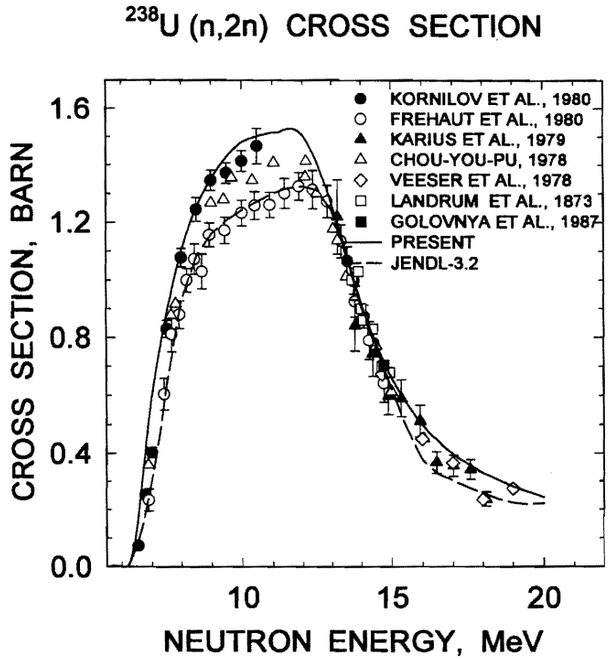

Fig. 61 (n,2n) cross section of ^{238}U.

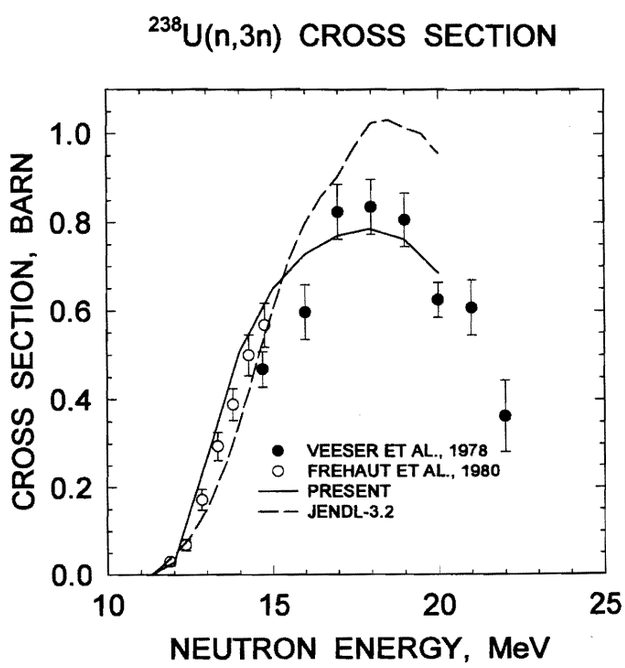

Fig. 62 (n,3n) cross section of ^{238}U.

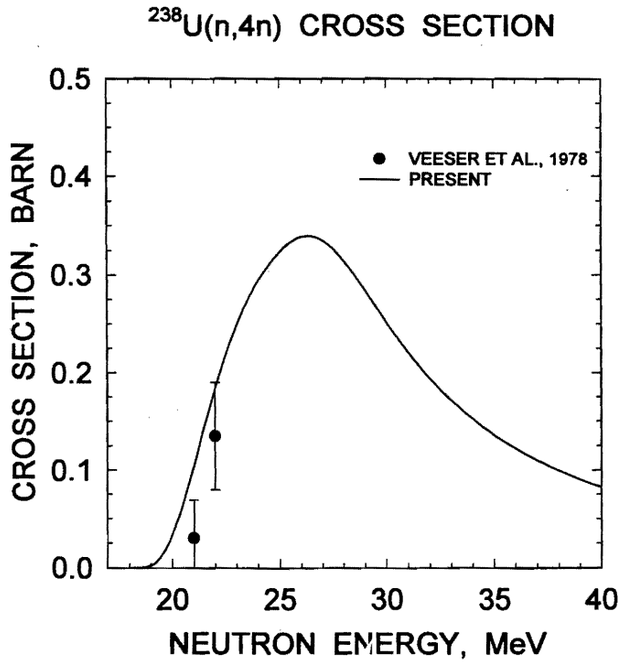

Fig. 63 (n,4n) cross section of ^{238}U.